Cell Chemical Biology

A Link between Linearmycin Biosynthesis and Extracellular Vesicle Genesis Connects Specialized Metabolism and Bacterial Membrane Physiology

Graphical Abstract
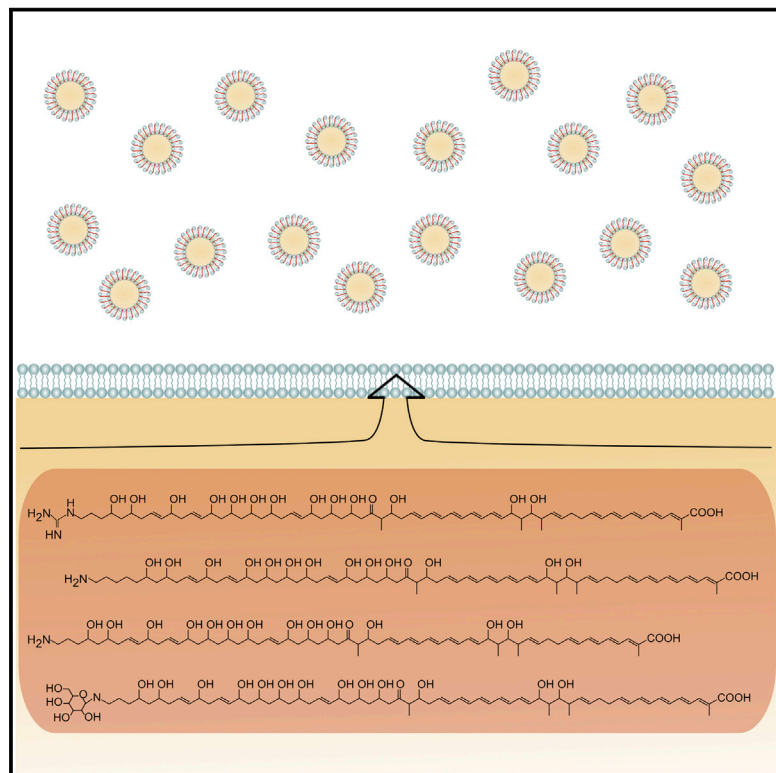
Authors

B. Christopher Hoefler,
Reed M. Stubbendieck,
N. Kalyani Josyula, Sabrina M. Moisan,
Emma M. Schulze, Paul D. Straight

Correspondence

paul_straight@tamu.edu

In Brief

Hoefler et al. describe a connection between linearmycin antibiotic biosynthesis and extracellular vesicle production by a species of *Streptomyces*. This connection provides an avenue to understand how a species of Gram-positive bacteria integrates these vital competitive functions.

Highlights

- A large family of linearmycin variants produced by a single assembly line

- Linearmycins are packaged into extracellular vesicles to deliver lytic activity

- Extracellular vesicle biogenesis is dependent on linearmycin biosynthesis

- Surfactin from *B. subtilis* enhances the lytic activity of linearmycins

CellPress

Article

A Link between Linearmycin Biosynthesis and Extracellular Vesicle Genesis Connects Specialized Metabolism and Bacterial Membrane Physiology

B. Christopher Hoefler,[1,3] Reed M. Stubbendieck,[1,2,3] N. Kalyani Josyula,[1] Sabrina M. Moisan,[1] Emma M. Schulze,[1] and Paul D. Straight[1,2,4,*]

[1]Department of Biochemistry & Biophysics, Texas A&M University, College Station, TX 77843, USA
[2]Interdisciplinary Program in Genetics, Texas A&M University, College Station, TX 77843, USA
[3]These authors contributed equally
[4]Lead Contact
*Correspondence: paul_straight@tamu.edu
http://dx.doi.org/10.1016/j.chembiol.2017.08.008

SUMMARY

Specialized metabolites support bacterial competitive fitness as antibiotics, signals, pigments, and metal scavengers. Little is known about how specialized metabolites are processed and trafficked for their diverse competitive functions. Linearmycins A and B are linear polyketides with antifungal and antibacterial activity but are colony-localized in imaging mass spectrometry of *Streptomyces* sp. Mg1 (*S.* sp. Mg1). To decipher a connection between colony localization and antibiotic activity, we identified the linearmycin gene cluster and investigated linearmycin production and distribution by *S.* sp. Mg1. Our results uncover a large family of variant linearmycins with limited solubility in aqueous solution. We hypothesized that extracellular vesicles may traffic the lipid-like linearmycins. We found that vesicles isolated from culture supernatants contained linearmycins. Surprisingly, abolishing production of linearmycins in *S.* sp. Mg1 also diminished extracellular vesicle production. Our results reveal integration of linearmycin biosynthesis with production of extracellular vesicles, suggesting a deep connection between specialized metabolism and bacterial membrane physiology.

INTRODUCTION

Specialized metabolism is a central feature of microbial competition and environmental adaptation (Raguso et al., 2015; Traxler and Kolter, 2015). While natural and therapeutic functions for a subset of specialized metabolites have been determined, the ecological functions of the vast majority of specialized metabolites are unknown. Models of microbial competition and environmental fitness demonstrate the relevance of antibiotics for producing organisms (Challis and Hopwood, 2003; Stubbendieck et al., 2016). However, specialized metabolites have other, diverse influences on microbial competition and environmental fitness. For example, chemical surfactants promote motility and development (Angelini et al., 2009; Branda et al., 2001; Caiazza et al., 2005; López et al., 2009), signaling molecules coordinate community functions (Waters and Bassler, 2005), and siderophores scavenge iron from the surrounding environment (Hider and Kong, 2010). The chemical and functional diversity encompassed by specialized metabolism suggests many undiscovered ecophysiological roles for these molecules.

One approach to discover specialized functions is to consider the spatial distributions of the metabolites. For instance, physical association of metabolites with the producing cells suggests possible localized functions. Examples of such metabolites include prodigiosins, which are tripyrrole-containing pigments produced by several bacterial species, including *Serratia marcescens* (Williams et al., 1956), and strains of *Streptomyces coelicolor* (Tsao et al., 1985) and *Streptomyces lividans* (Meschke et al., 2012). In addition to antibiotic activity, prodigiosins have several ascribed roles consistent with their cell-associated localization, including functions as antioxidants, UV protectants, and membrane proton shuttles (Borić et al., 2011; Gerber, 1975; Sato et al., 1998; Stankovic et al., 2012). A similar pattern of cell localization is observed for the antifungal metabolite amphotericin B (Baginski and Czub, 2009). A recent Raman spectroscopy imaging study of the producing organism, *Streptomyces nodosus*, showed a tight association of amphotericin B with the mycelium (Miyaoka et al., 2014). This localization pattern suggests possible producer-directed functions for amphotericin B and raises the question of how bacteria deliver amphotericin B and similarly localized metabolites as antibiotics in natural environments.

Extracellular vesicles are one mechanism of transport for hydrophobic and cell-associated specialized metabolites from bacteria. Outer membrane vesicles (OMVs) of Gram-negative bacteria carry toxic cargo as a competitive function. For example, *Pseudomonas aeruginosa* produces several hydrophobic virulence factors that are packaged into OMVs and function in competitive interactions (Kulp and Kuehn, 2010). As a component of OMV regulation, 2-heptyl-3-hydroxy-4-quinolone (PQS) is a quorum-sensing metabolite from *P. aeruginosa* that not only is packaged into vesicles, but functions in their formation as well (Mashburn-Warren et al., 2009; Schertzer and Whiteley, 2012). The connection between PQS and OMV formation demonstrates that some specialized metabolites play integrated

A

B
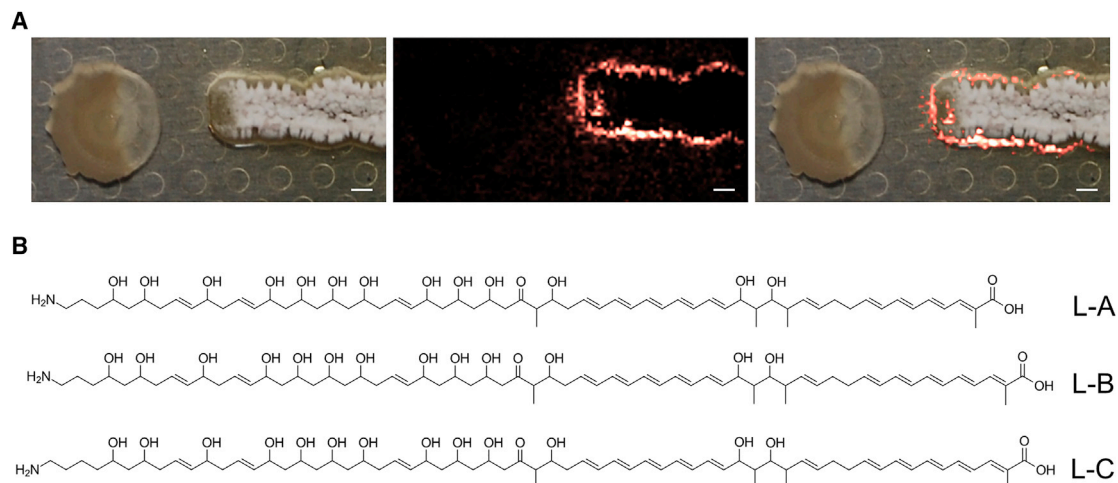
Figure 1. Linearmycin Family of Colony-Localized Specialized Metabolites

(A) Imaging mass spectrometry of bacterial competition between *B. subtilis* NCIB 3610 (left) and *S.* sp. Mg1 (right). Left: photograph of co-culture at 36 hr after inoculation. Center: extracted ion image of *m/z* 1,162. Right: overlay of the photograph with the extracted ion image. Scale bars, 1.5 mm.

(B) Chemical structures of the major linearmycin forms produced by *S.* sp. Mg1. Labels on the right correspond to linearmycin forms A and B (Sakuda et al., 1996), and C.

roles in lipid organization and OMV formation. The process of OMV formation by Gram-negative bacteria differs significantly from extracellular vesicle production by Gram-positive bacteria, which lack an outer membrane and build a substantially thicker peptidoglycan cell wall (Brown et al., 2015). Many species of Gram-positive bacteria, including *Bacillus subtilis* (Brown et al., 2014) and *Staphylococcus aureus* (Lee et al., 2009), generate extracellular vesicles. While the mechanisms of biogenesis are uncertain, extracellular vesicles are known in many cases to carry protein and metabolite cargo from the producer cell. For example, vesicles of *Streptomyces coelicolor* M110 have been shown to carry protein cargo and actinorhodin (Schrempf et al., 2011), and undecylprodigiosin associates with lipid vesicles produced by *Streptomyces lividans* (Schrempf and Merling, 2015).

In this report we focus on members of the linearmycin family of linear polyene polyketides. Linearmycins A and B were originally isolated from the mycelia of a *Streptomyces* sp. and characterized as antifungal and antibacterial compounds (Sakuda et al., 1996). Recently, our laboratory identified linearmycins, produced by *Streptomyces* sp. Mg1 (*S.* sp. Mg1), as diffusible lytic agents toward *B. subtilis* colonies (Stubbendieck and Straight, 2015). Paradoxically, we also found the linearmycins exhibit predominantly colony-associated localization when viewed by imaging mass spectrometry (Barger et al., 2012). To reconcile the seemingly contradictory patterns of cell localization and diffusible lytic activity, we used a combination of chemical and genetic approaches. We found that *S.* sp. Mg1 produces an extensive family of linearmycin variants. Based on the insolubility of purified linearmycins, we hypothesized an extracellular trafficking mechanism to deliver the lytic activity. Accordingly, we show that *S.* sp. Mg1 produces extracellular vesicles, and that linearmycin variants are components of the vesicles. Surprisingly, a linearmycin biosynthesis mutant was defective both for linearmycin production and extracellular vesicles. This unexpected

finding suggests an intrinsic role for linearmycins in the production of extracellular vesicles by *S.* sp. Mg1.

RESULTS

Identification of the Linearmycin Gene Cluster and Linearmycin C from *S.* sp. Mg1

We hypothesized that a colony-localized ion observed by imaging mass spectrometry (Barger et al., 2012) (Figure 1A) was a sodium adduct of linearmycin A (*m/z* 1,140 + Na$^+$ = *m/z* 1,162) (Sakuda et al., 1995). Extracts from a mycelial pellet of cultured *S.* sp. Mg1 revealed three major species with UV-absorption spectra consistent with linearmycins (Figure S1) (Sakuda et al., 1996). Tandem mass spectrometry (MS/MS) analysis agreed with the reported linearmycin A (*m/z* 1,140) and B (*m/z* 1,166) structures, and the third form appeared to be a previously unreported linearmycin (*m/z* 1,180) (Figure S1). To confirm the identity of *m/z* 1,180 as a linearmycin, we combined bioinformatic prediction with spectral analysis. From the completed genome of *S.* sp. Mg1 (GenBank: CP011664.1) (Hoefler et al., 2013), we identified based on the size, ~180 kb, and similarity to the gene cluster for ECO-02301 (McAlpine et al., 2005), a type I polyketide synthase (PKS) gene cluster as the primary candidate gene cluster for biosynthesis of linearmycins in *S.* sp. Mg1 (Table S3), which has not been previously reported.

We propose a biosynthetic scheme for linearmycins by analysis of the domain organization of the PKS genes and surrounding open reading frames (Figure S2). Biosynthesis-guided interpretation of high-resolution 1D and 2D nuclear magnetic resonance (NMR) data resolved overlapping peaks from degenerate parts of the molecules (Table S4). We obtained a complete structural assignment of the *m/z* 1,180 metabolite (Figure S2), which we name linearmycin C, and confirmed the structures of the *m/z* 1,140 and *m/z* 1,166 variants by differential NMR analysis as linearmycins A and B, respectively (Figure 1). Two
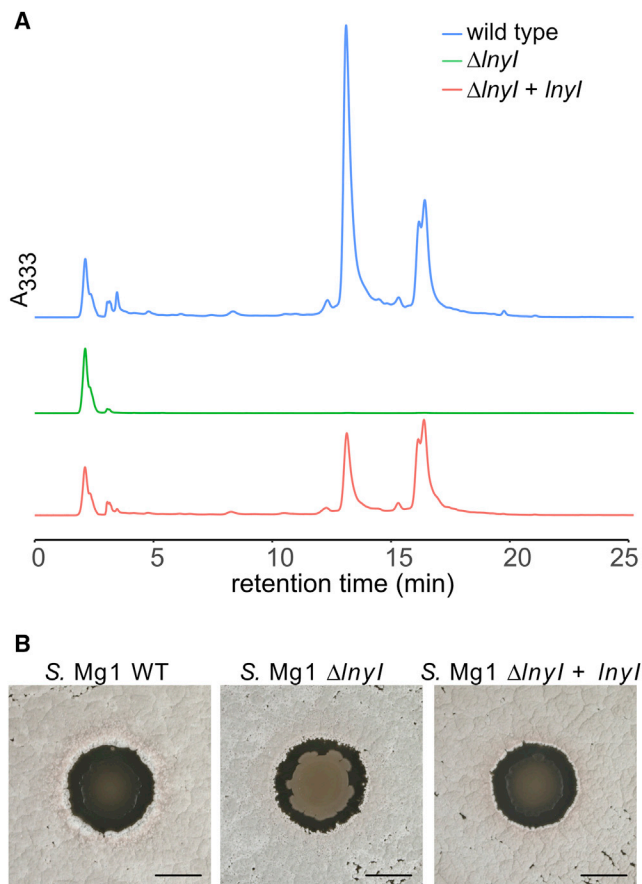
Figure 2. Disruption of the *Iny* Gene Cluster Blocks Linearmycin Production and Lytic Activity

(A) HPLC chromatograms (UV, A_{333}) of extracts from wild-type, Δ*InyI*, and *InyI* complement *S.* sp. Mg1. The 13 min peak corresponds to linearmycin A and peaks at 16 min to linearmycins B and C.

(B) Photographs of the corresponding *S.* sp. Mg1 strains co-cultured with *B. subtilis* 3610 to monitor the lysis phenotype. Lysed colonies of *B. subtilis* are transparent when surrounded by linearmycin producers, but remain opaque with *S.* sp. Mg1 Δ*InyI*. Scale bars, 1 cm. HPLC and lytic assays were repeated a minimum of two times with consistent results.

structural features differentiate linearmycins A, B, and C, the incorporation of a distinct starter unit and the length of the terminal polyene (Figure 1B). The aminopentanoic acid starter unit of linearmycin C is a single-methylene extension of the starter unit of linearmycins A and B, indicating that starter unit biosynthesis can accommodate different substrates. Linearmycin A, when compared with linearmycin B, is missing a single olefin in the terminal polyene chromophore, suggesting a skipped module during synthesis.

Deletion of *InyI* Disrupts Linearmycin Production and Lytic Activity

To confirm the assignment of the linearmycin gene cluster (*Iny*) and to identify loss-of-function phenotypes, we genetically disrupted production of the three identified linearmycin metabolites. We engineered a targeted deletion of the predicted acyltransferase (*InyI*, Table S3) likely required for initiation of linearmycin

biosynthesis. The acyltransferase open reading frame was replaced with an apramycin resistance marker by homologous recombination and the replacement location was confirmed. Using the *InyI* mutant, we observed by high-performance liquid chromatography (HPLC) that no linearmycins were produced (Figure 2A). The absence of all linearmycins in the *InyI* mutant strain confirmed the assignment of the *Iny* gene cluster. To complement the *InyI* deletion, a second strain was created by reintroduction of the wild-type *InyI* gene, under the control of its native promoter, into the *attB* phage attachment site. When *InyI* was reintroduced by genetic complementation, linearmycin production by *S.* sp. Mg1 was restored, although a slight reduction in linearmycin A relative to other forms was observed (Figure 2A). Since linearmycins cause lysis of *B. subtilis* (Stubbendieck and Straight, 2015), we tested the mutant phenotype using competitive culture. We observed lysis using wild-type and *InyI*-complemented strains, but not using the *InyI* mutant strain. The results confirm that the *InyI* mutation disrupts linearmycin biosynthesis specifically, and that linearmycins are the sole agents of lysis in our biological assays of competition (Figure 2B).

Linearmycins Are Composed of a Large Family of Structural Variants

In addition to linearmycins A, B, and C, the HPLC and liquid chromatography (LC)-MS chromatograms of extracts from Δ*InyI* *S.* sp. Mg1 were missing several minor peaks present in wild-type extracts (Figures 2A and S3). The differences in the spectra raised the possibility of *S.* sp. Mg1 producing additional forms of linearmycins not represented by the three characterized molecules. To obtain a broad view of potential linearmycin derivatives in our extracts, we used a mass spectral molecular networking approach (MS/MS networking) (Nguyen et al., 2013; Watrous et al., 2012). When applied to extracts from Δ*InyI* and wild-type *S.* sp. Mg1, MS/MS networking revealed large families of metabolites that cluster into separate sub-networks based on structural similarity (Figures 3A and S4). We used network visualization tools to separate metabolites into groups based on strain origin and estimated the relative abundance and similarity between variants. Our network analysis of the extracts allowed us to identify clusters of metabolites that were clearly related to linearmycins and to differentiate them from the other metabolites present.

To our surprise, we uncovered over 50 potential structural variants of linearmycins produced by *S.* sp. Mg1 beyond the three major forms that we isolated. Analysis of the MS/MS spectra of the variants allowed us to identify some of the modifications and place separate variants into classes (Figures 3B, S5, and S6). One class is composed of biosynthetic variants that likely arise from deviations or disruptions on the PKS assembly line. For example, *m/z* 1,126 (Figure S5A) appears to result from premature chain termination, and *m/z* 1,152 (Figure S5B) from substitution of malonyl-coenzyme A (CoA) for methylmalonyl-CoA. A second class of variants appears to arise from PKS-independent tailoring modifications. The aminobutanoic acid starter unit of linearmycins A and B is proposed to originate from arginine (McAlpine et al., 2005). In our extracts, the *m/z* 1,208 variant (Figure S6A) retains the guanidino moiety of arginine, consistent with starter unit processing similar to that observed for other antifungal metabolites (Hong et al., 2013). As previously noted, the
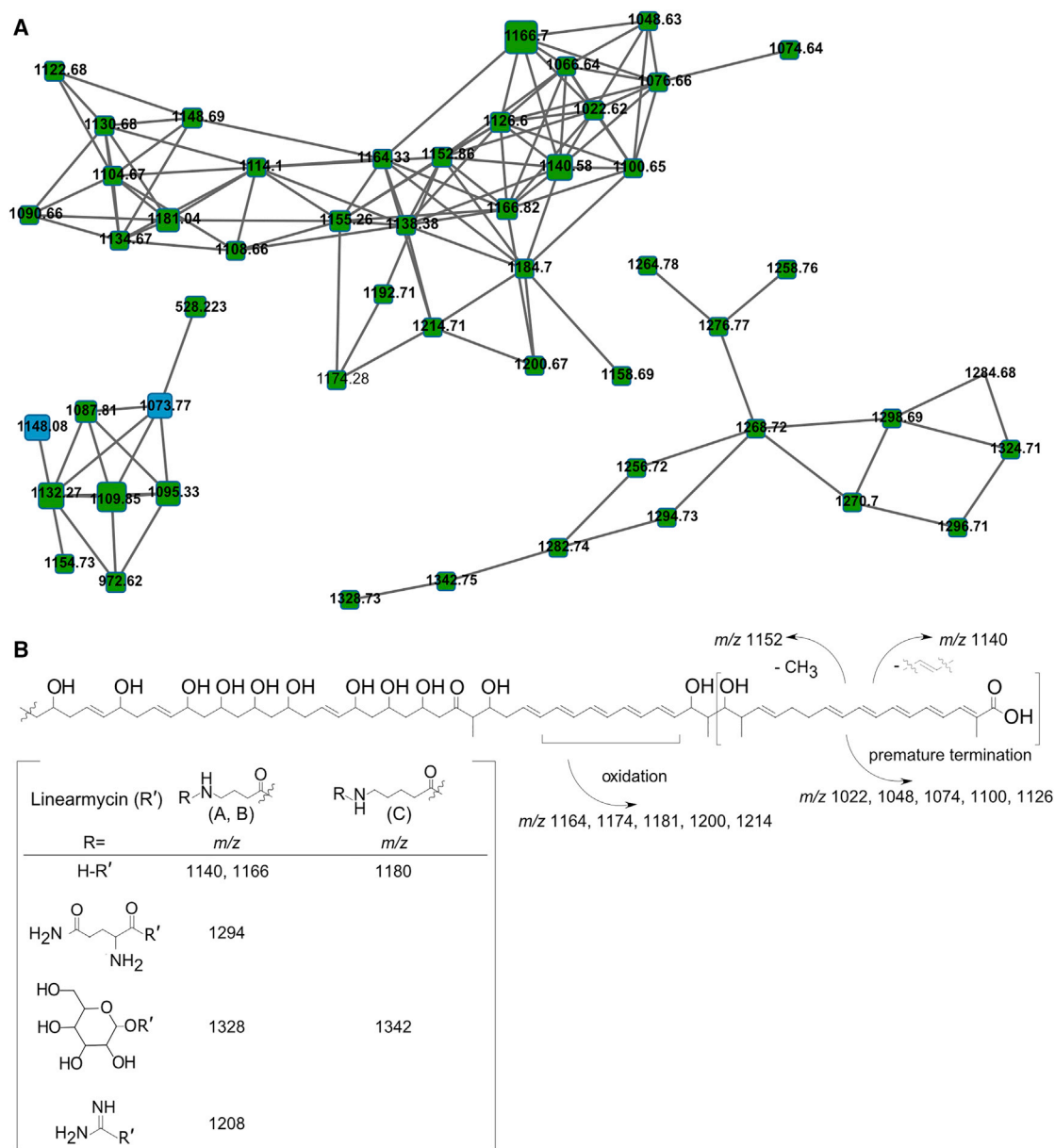
Figure 3. Clusters of High Similarity-Scoring Linearmycin Variants from MS/MS Networking of Wild-Type and Δ*lnyI* *S.* sp. Mg1 Extracts

(A) Linearmycin variants that cluster by similarity with the major isolated linearmycin forms A, B, and C, and two sub-clusters of linearmycin variants that are more structurally divergent from the major forms. Each node represents one MS1 precursor ion. Ions observed only in the wild-type extract are colored green, and those in wild-type and Δ*lnyI* are blue. Nodes are connected if their MS/MS similarity has a cosine score of 0.85 or greater. Node sizes are scaled relative to the precursor ion intensity. Inspection of MS/MS spectra indicated that blue nodes in the Δ*lnyI* extracts result from spurious data-dependent precursor selection within low signal-to-noise spectra.

(B) Several linearmycin variants produced by *S.* sp. Mg1 as predicted from MS/MS networking and fragment mass analysis.

extended starter unit for biosynthesis of linearmycin C suggests that the biosynthetic enzymes are able to accommodate alternate substrates as well. We detected apparent additions of glutamine to the amine of the starter unit (*m/z* 1,294) (Figure S6B), as well as glycosylation (*m/z* 1,342) (Figure S6C). Also, we detected products (e.g., *m/z* 1,200) of mass consistent with oxidation of linearmycins (Figure S6D). In these cases, because the gene cluster lacks candidate-tailoring enzymes, the mechanisms of synthesis for these modifications are currently

unknown. Collectively, the observed structural variants of linearmycins suggest that the molecules form a diverse family of colony-associated polyenes, which are secreted in a solubilized form to function as lytic agents.

Linearmycins Associate with Extracellular Vesicles of *S.* sp. Mg1

We next sought to understand how colony-associated linearmycins dissociate from the *S.* sp. Mg1 colony to function as

diffusible lytic agents. During purification of linearmycins A, B, and C we found the molecules have a propensity to aggregate in aqueous solution. In bacteria, extracellular vesicles and bio-surfactants such as rhamnolipids and lipoproteins can provide transport mechanisms for otherwise insoluble cargo (Brown et al., 2015; Cortés-Sánchez Ade et al., 2013; Mashburn and Whiteley, 2005). We hypothesized that extracellular vesicles would serve to transport linearmycins from the producing cells. To detect extracellular vesicles, we subjected the cell-free supernatants of liquid cultures to ultracentrifugation. Pelleted material from the supernatant was examined by electron microscopy (EM) using a negative stain to enhance detection of membrane structures (Figure 4A). Consistent with vesicle formation, we observed vesicular structures with a size range of ~75–200 nm in diameter.

To determine whether the vesicles were trafficking linearmy-cins, we fractionated the crude vesicle preparation in an iodixa-nol gradient to separate vesicles from aggregates and other cellular debris (Figures S7A and SB). The buoyant fractions with the majority of the vesicles were analyzed by LC-MS. Line-armycins were detected in the fractions, which included all three of the major forms and many of the variants (Figure 4B). The presence of linearmycins in the vesicles, in addition to their lytic activity toward *B. subtilis*, leads us to propose that vesicle forma-tion by *S.* sp. Mg1 serves to traffic linearmycins from the colony surface to the external environment. Linear polyene metabolites are produced by other species of *Streptomyces*, including ECO-02301 from *Streptomyces aizunensis* (McAlpine et al., 2005). To determine whether association of vesicles with linear polyenes is unique to *S.* sp. Mg1 and linearmycins, we similarly fractionated the cell-free supernatant of an *S. aizunensis* culture and exam-ined the material by EM and MS (Figures S7D–SF). Extracellular vesicles were present in fractions that contained ECO-02301, consistent with packaging of a linear polyene into vesicles by a species other than *S.* sp. Mg1. We also observed many tubular structures in addition to typical vesicles in the *S. aizunensis* sam-ples. Although the basis for differences in morphology is not currently known, the presence of ECO-02301 and extracellular vesicles indicates an association of vesicles and linear polyketi-des is not unique to *S.* sp. Mg1.

The *lnyI* Mutation Disrupts Extracellular Vesicle Formation

In parallel with our wild-type samples, we prepared vesicles from cell-free supernatants of Δ*lnyI S.* sp. Mg1 liquid cultures, antici-pating that vesicles from the mutant would be devoid of linear-mycins. We were surprised to discover greatly diminished vesicle production in the mutant samples. By comparison of EM micrographs from pelleted supernatants of the wild-type control, pellets from the Δ*lnyI* strain showed few vesicle-like bodies, but instead exhibited relatively small, opaque aggre-gates and disorganized structures (Figures 4C, 4D, S7A, and S7B). To confirm that the change in vesicle formation was a result of linearmycin disruption in *S.* sp. Mg1, and not a pheno-type from an unrelated mutation, we isolated vesicles from the *lnyI* complement strain. We observed restored vesicle produc-tion upon EM analysis of these samples (Figures 4E, S7A, and S7B), indicating that linearmycin biosynthesis is required for proper vesicle biogenesis by *S.* sp. Mg1.

To obtain a quantitative assessment of the vesicle-deficient phenotype, we counted vesicle bodies visible by EM of multiple samples from wild-type and Δ*lnyI* strains, and we measured the cross-sectional area of the vesicles counted (Figures 4F–4H). The analysis of 1,413 total apparent vesicles revealed a ratio of 0.27 vesicle-like bodies for Δ*lnyI*/wild-type. The distorted shape and staining of apparent vesicle-like bodies in the Δ*lnyI* samples suggests that the 0.27 ratio is a conservative measure of the vesicle biogenesis defect (Figure 4G). *Streptomyces lividans* has been reported to produce two classes of vesicles based on their relative size (Schrempf et al., 2011). For *S.* sp. Mg1, the Δ*lnyI* mutant samples showed a prominent loss of smaller vesicles (<100 nm diameter based on the measured cross-sectional area) (Figure 4H). The presence of linearmycins in extracellular vesicles and the dependence of vesicle biogenesis on linearmycin biosynthesis suggest a direct connection be-tween the specialized metabolism of a polyketide and lipid mem-brane functions of *S.* sp. Mg1.

Coordinated Production of Linearmycins and Extracellular Vesicles in *S.* sp. Mg1

We hypothesized that *S.* sp. Mg1 coordinates linearmycin biosynthesis with extracellular vesicle production during its life cycle. To determine the profile of linearmycin gene expres-sion and production of linearmycin-carrying extracellular vesi-cles, we first monitored cell density during growth of *S.* sp. Mg1 in liquid culture and sampled the cultures at indicated times (Figure 5). Concurrently, we extracted RNA from the cell pellets to measure expression of the *lny* genes, and we sampled the cell-free culture supernatants for extracellular vesicles and linearmycins. The growth curve of *S.* sp. Mg1 re-vealed a pattern typical of other streptomycetes cultured in rich medium (Manteca et al., 2008), wherein a transient pause in growth occurs between spore germination and stationary phase (Figure 5A). We monitored by quantitative RT-PCR the abundance of *lnyHA* and *lnyHI* transcripts, located respectively at the beginning and end of the ~150 kb assembly line-encod-ing genes. We report the changes in gene expression relative to the earliest time (24 hr) where growth was observed (Figures 5B and S7C). The *lnyHA* and *lnyHI* transcripts increased 14-fold in abundance from 24 to 48 hr and subsequently declined in stationary phase, consistent with a regulated pattern of linear-mycin production.

We monitored the production of extracellular vesicles and linearmycins by fractionating the pellets from cell-free superna-tants at each time point to isolate vesicles. Fractions from wild-type and Δ*lnyI* strains were spotted onto lawns of *B. subtilis* to monitor cell lytic activity. As seen in Figure 6A, vesicle-associated lytic activity was highest in fractions 5 and 6. The lytic activity of vesicles was detectable as early as 24 hr after inoculation of cultures. At subsequent times, the 5 and 6 fractions were saturated with linearmycin activity, which enabled us to measure the relative activity at each time. We compared the lytic activities of serial dilutions from pooled fractions 5 and 6 for each time point from 24 to 96 hr (Figure 6B). The lytic concentra-tion of linearmycins (LC_{50}) in the vesicle fractions increased over time, in accord with direct measurements of linearmycins abun-dance by HPLC (Figure 6C). In contrast to wild-type, the *lnyI* mutant strain did not produce linearmycins or exhibit lytic activity
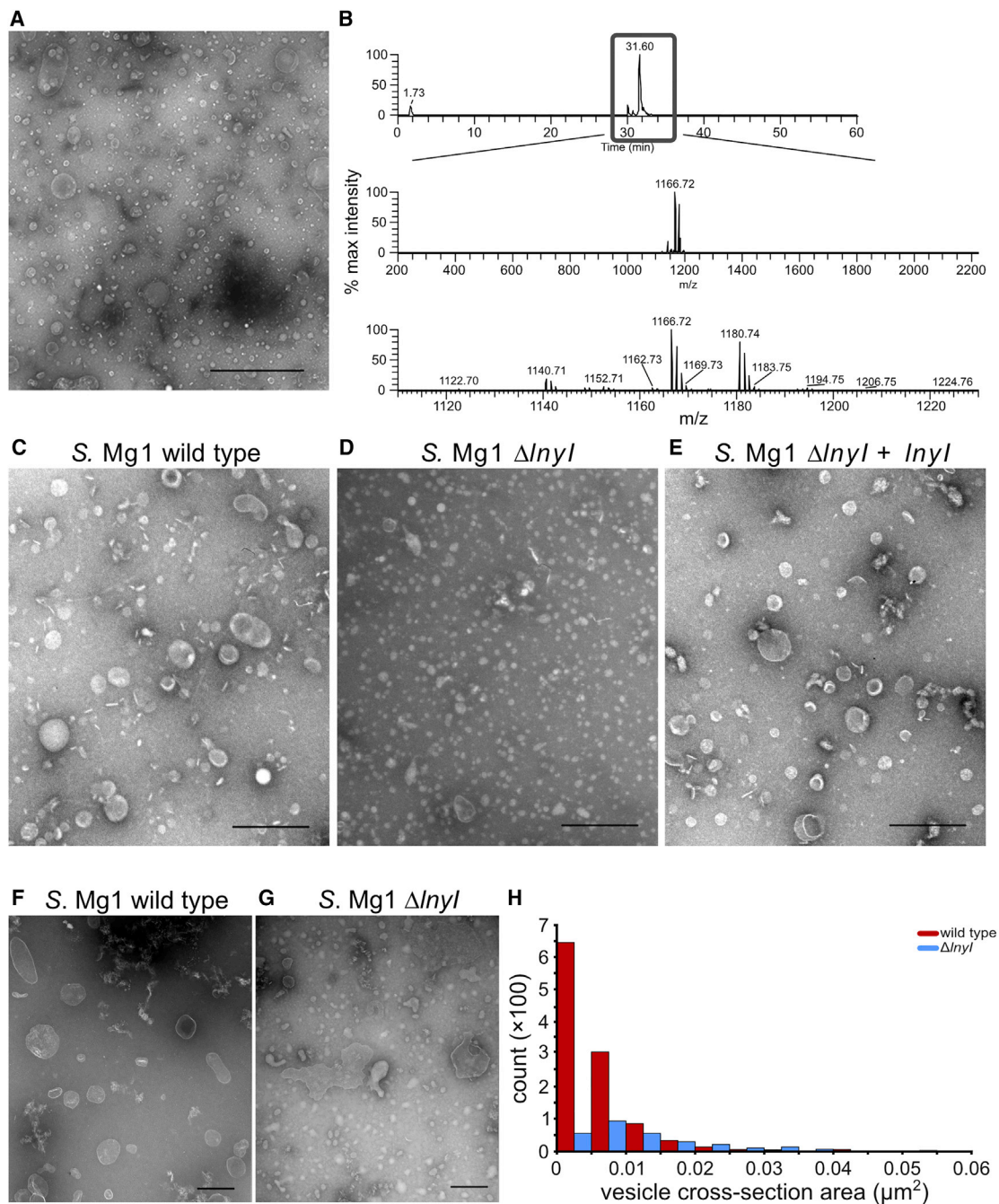
Figure 4. Extracellular Vesicles Isolated from Culture Supernatants of *S.* sp. Mg1

(A) EM of negative-stained extracellular vesicles collected from wild-type *S.* sp. Mg1 supernatant. Scale bar, 1 μm.

(B) LC-MS analysis of fractionated vesicles produced by *S.* sp. Mg1. Upper: LC-retention time of linearmycins. Middle: extended range (200–2,200 *m/z*) of major peaks in LC-MS. Lower: expanded range from 1,110 to 1,230 *m/z* to identify major forms of linearmycins detected. The three major linearmycin forms A, B, and C have the highest peak intensity relative to other forms.

(C–E) EM micrographs from wild-type (C), Δ*lnyI* (D), and *lnyI* complement (E) pelleted supernatants for vesicle fractionation. Scale bars, 0.5 μm.

(F–H) Quantitation of Δ*lnyI* vesicle biogenesis defect. (F) Representative EM of negative-stained vesicle preparations from pooled supernatant fractions 5 and 6 (relates to Figure 6) from (F) wild-type and (G) Δ*lnyI S.* sp. Mg1 strains. Scale bar, 0.2 μm. (H) A histogram of 1,413 vesicle counts sorted by vesicle cross-sectional area (μm²) from two independent biological replicate experiments. Relates to Figure S7 (A and B).
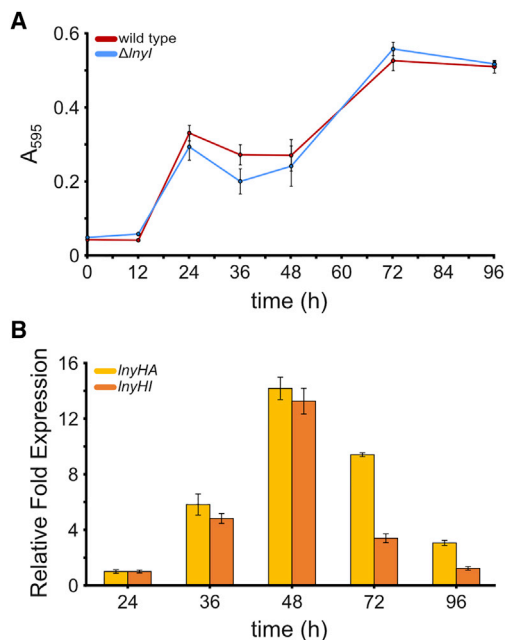
Figure 5. *Streptomyces* sp. Mg1 Growth, Linearmycin Biosynthesis, and EV Production

(A) Growth curve of *S.* sp. Mg1 wild type and Δ*lnyI* mutant measured by a diphenylamine colorimetric assay (Zhao et al., 2013). Each time point was measured ≥ 3 times and the error bars represent the SD of the measurements. A pause in growth occurs between 24 and 48 hr, similar to an observed pause in *S. coelicolor* liquid cultures (Manteca et al., 2008).

(B) Quantitative RT-PCR of *lnyHA* and *lnyHI* from *S.* sp. Mg1 wild type at the specified time points. The error bars represent the SD of the fold difference. Relates to Figure S7C.

at any stage of growth, and the fractions were diminished in vesicle abundance as observed by EM (Figures 4F–4H).

Surfactin Enhances Linearmycin Sensitivity of *B. subtilis*

Our experimental results reveal a temporal profile of linearmycin production by *S.* sp. Mg1 cultured in isolation. In the course of this work, we did not observe any effect of the competitor *B. subtilis* on linearmycin biosynthesis. However, *B. subtilis* produces surfactin, a lipopeptide surfactant previously demonstrated to disrupt extracellular vesicles of *B. subtilis* and *Bacillus anthracis* (Brown et al., 2014). We questioned whether surfactin would destabilize linearmycin-carrying vesicles and influence their lytic activity toward *B. subtilis*. For this experiment, we used a Δ*srfAA* strain of *B. subtilis*, which does not produce surfactin. We isolated vesicle-containing fractions from the 24-hr *S.* sp. Mg1 samples, and applied the vesicles to lawns of *B. subtilis* Δ*srfAA* and wild-type strains (Figure 7A). Comparison of the results revealed that, relative to wild type, the Δ*srfAA* strain is more resistant to lysis by linearmycin-carrying vesicles. The addition of purified surfactin restored the lytic activity (Figure 7B). Intriguingly, we observed enhanced lytic activity with the surfactin-treated mutant strain over that observed with the untreated wild-type strain. The hypersensitivity could arise from solubilized linearmycins, or, alternatively, could be due to a secondary effect of surfactin on the Δ*srfAA* mutant strain (López et al., 2009; Ut-

tlová et al., 2016). In either case, surfactin appears to enhance the lytic activity of linearmycins toward *B. subtilis*, possibly through a combination of vesicle disruption and surfactin-enhanced solubility of linearmycins.

DISCUSSION

Linearmycins are part of an expanding family of linear polyene metabolites produced by streptomycetes, many of which are demonstrated antifungal and antibacterial compounds. This family includes ECO-02301, clethromycins, and mediomycins, which are produced by different species of *Streptomyces* (Cai et al., 2007; Igarashi et al., 2003; McAlpine et al., 2005). These metabolites share similar, but non-identical, polyene scaffolds, which include various tailored forms. Examples of tailoring differences include methylation, glycosylation, sulfation, and substitution of different starter units, among others. Considered collectively, linear polyenes represent a variable class of polyketide natural products. We found that *S.* sp. Mg1 alone produces a large number of linearmycin variants that associate with colonies and with extracellular vesicles.

When combined with analysis of the domain organization in the biosynthetic gene cluster, some specific variations in linearmycin structure suggest a mechanistic basis for their formation. For instance, both linearmycin A and B terminate with an α-methyl branched carboxylic acid, arising from incorporation of methylmalonyl-CoA in the final module of *lnyHI*. The presence of the identical final unit in linearmycins A–C indicates a module-skipping mechanism for biosynthesis of linearmycin A, as opposed to premature chain termination. Similar module-skipping mechanisms have been observed for other polyketides, such as pikromycin, where skipping of the final PKS module produces a 12-membered instead of a 14-membered macrolactone product (Xue and Sherman, 2000). In addition, salinipyrone biosynthesis was recently proposed to require module skipping on the rosamicin biosynthetic gene cluster (Awakawa et al., 2015). Module skipping and domain skipping as methods for generating polyketide diversity may be more widespread than previously recognized. Other linearmycins arise from apparent variations in the starter unit used. Structural congeners of linearmycins A and B resemble clethramycins, which incorporate 4-guanidinylbutyrate derived from arginine as a starter unit (Hong et al., 2013). Linearmycins A and B are likely to follow the same mechanism of starter unit biosynthesis, followed by conversion to a primary amine through the action of an agmatinase encoded in the gene cluster (*lnyT*). Linearmycin C, however, uses an extended starter unit, the origin of which cannot be inferred from the gene cluster. Overall, the diversity of products may reflect the inherent stochasticity expected of a long PKS assembly line (encoded by an ∼150 kb operon) accompanied by additional proteins required for regulation, export, tailoring, and starter unit biosynthesis. As clear candidates for tailoring enzymes are not encoded within the gene cluster, understanding the mechanistic basis for several linearmycin modifications and their functional significance will require further study.

The large number of variants, along with cellular localization, suggests that the linearmycins form a PKS-derived family of cellular lipids. How linearmycins physically associate with cells
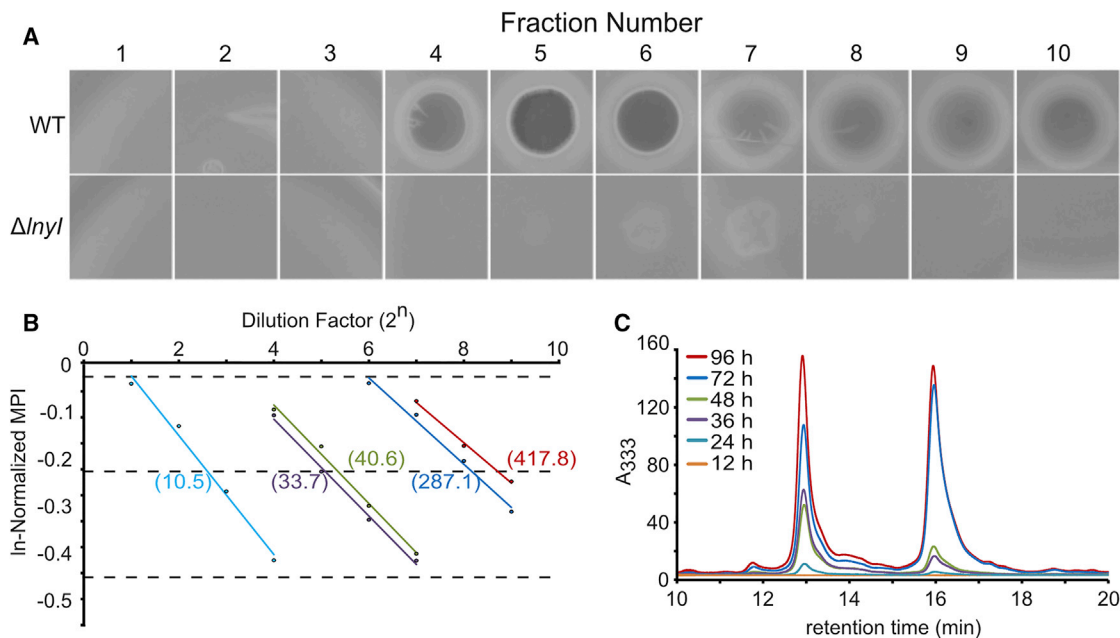
Figure 6. Quantitation of Vesicles from Fractionated Wild-Type and ΔlnyI Supernatants

(A) Example activity assay used to detect the presence of linearmycin-carrying vesicles from a culture of *S.* sp. Mg1 grown for 24 hr. Lysis is indicated by a zone of clearing when 3 μL of a vesicle fraction was spotted onto a high-density lawn of *B. subtilis*. Fraction numbers are indicated above each panel and range from 0% to 50% iodixanol in a continuous gradient. Fractions 5 and 6 were the most active and were used for related experiments.

(B) Graph of mean pixel intensity (MPI, see STAR Methods) versus dilution factor for pooled fractions 5 and 6 from vesicle preparations. Line colors indicate the times of sampling (24–96 hr) as in (C). Numbers in parentheses indicate the calculated LC_{50} dilution factors for each sample.

(C) HPLC chromatograms (UV, A_{333}) of fractions 5 and 6 that were pooled and extracted with an equal volume of methanol.

and with extracellular vesicles is unknown, although a provocative model involves the direct insertion of linearmycins into phospholipid bilayers. Alternatively, linearmycins could be either sequestered on the interior of phospholipid vesicles, associated with cell wall materials on the exterior, or they could assemble themselves into vesicle-like bodies as they are synthesized and secreted by *S.* sp. Mg1. Linearmycins are not the only linear polyenes to be associated with extracellular vesicles. For instance, the myxalamids of *Myxococcus xanthus* are another example, yet how they are inserted into vesicles is also not known (Berleman et al., 2014). An exciting but unexplored prospect is whether other metabolites, which share chemical and structural properties with linearmycins, are also packaged integrally with vesicle biogenesis. As an initial observation, we have shown that ECO-02301, which is structurally similar to linearmycins, is associated with extracellular vesicles of *S. aizunensis*.

Bacterial extracellular vesicles are an established mechanism for transporting protein and small-molecule cargoes from bacteria (Brown et al., 2015; Schwechheimer and Kuehn, 2015). The detailed process of extracellular vesicle formation is likely to vary with the originating organism. In the coarsest distinction, Gram-negative bacteria generate vesicles from the outer membrane, whereas Gram-positive bacteria must use a different mechanism. Despite their presence in cultures of many Gram-positive species, including *S. aureus* (Lee et al., 2009), *Listeria monocytogenes* (Lee et al., 2013), *Mycobacterium tuberculosis* (Prados-Rosales et al., 2011), and species of *Streptomyces*

(Schrempf and Merling, 2015; Schrempf et al., 2011), it remains unclear how Gram-positive extracellular vesicles form and cross the cell wall peptidoglycan to reach the outside of the cell. Proposed mechanisms such as protein channels, peptidoglycan remodeling, and turgor pressure-driven extrusion are non-mutually exclusive pathways of extracellular vesicle production, but a single mechanism is yet to be established (Brown et al., 2015). One challenge to the study of extracellular vesicles in Gram-positive organisms is the lack of any known null mutants in the studies reported. Although the ΔlnyI phenotype of *S.* sp. Mg1 is also not null for vesicle formation, the connection between linearmycin synthesis and vesicle biogenesis provides a new avenue for better understanding vesicle formation. For example, the linearmycins could be tracked from synthesis to vesicle packaging as a unique signal upon which normal vesicle biogenesis depends.

Streptomycetes are distinctive in their growth as filamentous mycelia, a morphology shared with filamentous fungi. A mycelium may provide a specialized structure to support formation of vesicles. For instance, programmed cell death occurs within the mycelia of *S. coelicolor* cultured in liquid medium, and the onset of lysis occurs shortly after establishment of mycelial masses (Manteca et al., 2008). One possibility is that programmed cellular lysis releases intracellular vesicles into the environment. Indeed, this mechanism has been recently reported within colonies of the Gram-negative species, *P. aeruginosa* (Turnbull et al., 2016), and may be available to a wide range of organisms that build communities and biofilms. Another intriguing possibility exists for coordination between
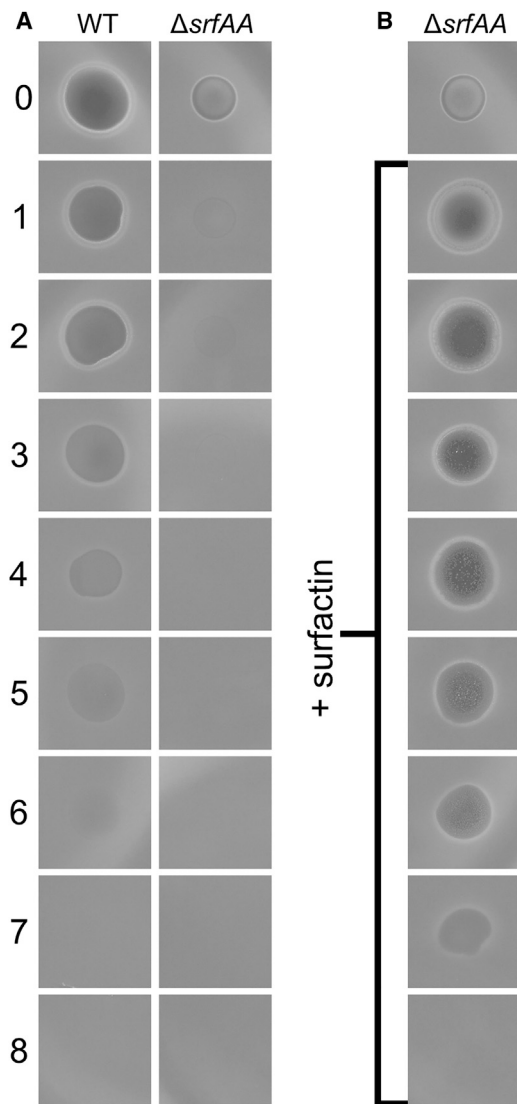
Figure 7. Surfactin Enhances Linearmycin Sensitivity of *B. subtilis*

(A) High-density lawns of both Δ*srfAA* and wild-type strains of *B. subtilis* NCIB 3610 were treated with serial dilutions of pooled fractions 5 and 6 containing linearmycins from a 24 hr culture of *S.* sp. Mg1. Lysis is indicated by a zone of clearing.

(B) High-density lawns of the Δ*srfAA* strain of *B. subtilis* NCIB 3610 were treated with serial dilutions of pooled vesicle fractions 5 and 6 from a culture of *S.* sp. Mg1 grown for 24 hr that were pre-treated with 2.5 mg/mL of surfactin before being spotted. The numbers indicate the dilution factor $[(1/2)^n]$ for each panel.

cell morphologies, the mechanisms of extracellular vesicle formation are likely to vary and be tailored to the specialized needs of the producing organisms.

Specialized metabolites are key components of the competitive fitness of many bacteria. We have shown that linearmycins, similar to other metabolites such as amphotericin B, are localized to the cell surface, possibly embedded in the membranes of the producing bacteria. What functions the metabolites may convey in their cell-associated compartments are unknown. However, the linearmycins undergo packaging into extracellular vesicles, which enable delivery to a competitor, *B. subtilis*. In competition with *B. subtilis*, vesicle-mediated delivery may have particular advantages. Surfactin is required for swarming and sliding motility and biofilm formation by *B. subtilis* (Branda et al., 2001; Kearns and Losick, 2004; Kinsinger et al., 2003). Packaging linearmycins into vesicles may provide a competitive advantage to *S.* sp. Mg1 by exploiting surfactin to aid the delivery of the lytic agents. We suspect that surfactins disrupt the vesicles at or near the *B. subtilis* cells and possibly help to solubilize linearmycins. However, *S.* sp. Mg1 also produces surfactin hydrolase, which would counteract the effect of surfactin on extracellular vesicles (Hoefler et al., 2012). These observations expose the complexity of chemical interactions in the spaces between bacteria, which determine the fates of competitors, and possibly the structures of microbial communities.

SIGNIFICANCE

Bacteria produce structurally diverse specialized metabolites, many of which are medically useful natural products. Specialized metabolites are likely to have vital functions for the producer organisms in natural environments, but the natural functions for most of these molecules are not known. This study focuses on linearmycins, which are produced by some species of *Streptomyces* and have antibiotic activity toward some fungi and bacteria. We report the discoveries that many structurally diverse linearmycins are trafficked by extracellular vesicles, and that linearmycin biosynthesis and extracellular vesicle biogenesis are functionally linked in *Streptomyces* sp. Mg1. A linearmycin-deficient strain of *Streptomyces* sp. Mg1 is defective for production of extracellular vesicles. These results uncover a deep integration of natural product biosynthesis with the physiology of cellular membranes. Although mechanistic details await discovery, our findings provide new tools for dissection of both extracellular vesicle biogenesis and a producer-directed natural function for linearmycins.

STAR★METHODS

Detailed methods are provided in the online version of this paper and include the following:

- KEY RESOURCES TABLE
- CONTACT FOR REAGENT AND RESOURCE SHARING
- EXPERIMENTAL MODEL AND SUBJECT DETAILS
  - Bacterial Strains, Primers, and Media

lipid biosynthesis and specialized metabolite biosynthesis, whereby lipid and specialized metabolite export functions, which remain poorly understood, become intertwined. A recent study of *Aspergillus* demonstrated the coupled synthesis of melanin pigments by PKS enzymes associated with intracellular vesicles, which transport the pigments to the cell membrane for export (Upadhyay et al., 2016). Although this coupling may serve to deliver metabolites to the membrane, the challenge for extracellular vesicles to cross cell wall structures remains unanswered. Given the diversity of Gram-positive cell wall structures and

- **METHOD DETAILS**
  - Extraction and Purification of Linearmycins
  - Accurate Linearmycin Mass Determination
  - MS/MS of Linearmycins
  - UV-Vis Measurements of Linearmycins
  - NMR Analysis of Linearmycins
  - Linearmycin Gene Cluster Analysis
  - Cosmid Library Preparation and *lny* Gene Cluster Identification
  - Mutagenesis of *lnyI* and Genetic Complementation
  - Co-culture Plates
  - Extraction of *S.* Mg1 Metabolites from Agar Plates
  - LC-MS for MS/MS Networking of *S.* Mg1 Metabolites
  - MS/MS Network Construction
  - Isolation of Vesicles
  - EM of Vesicles
  - LC-MS Analysis of Vesicles
  - Time Course Experiment
  - Growth Measurements
  - Time Course Vesicle Extraction, Purification, and EM
  - Plate Overlay Lysis Assays and LC_{50} Measurement
  - Quantification of Linearmycin in Vesicle Preparations
  - RNA Extraction and Cleanup
  - Quantitative RT-PCR
  - Vesicle Quantitation
  - Surfactin Test
- **QUANTIFICATION AND STATISTICAL ANALYSIS**

REFERENCES

Anand, S., Prasad, M.V.R., Yadav, G., Kumar, N., Shehara, J., Ansari, M.Z., and Mohanty, D. (2010). SBSPKS: structure based sequence analysis of polyketide synthases. Nucleic Acids Res. *38*, W487–W496.

Angelini, T.E., Roper, M., Kolter, R., Weitz, D.A., and Brenner, M.P. (2009). *Bacillus subtilis* spreads by surfing on waves of surfactant. Proc. Natl. Acad. Sci. USA *106*, 18109–18113.

Awakawa, T., Crüsemann, M., Munguia, J., Ziemert, N., Nizet, V., Fenical, W., and Moore, B.S. (2015). Salinipyrone and pacificanone are biosynthetic by-products of the rosamicin polyketide synthase. ChemBioChem *16*, 1443–1447.

Baginski, M., and Czub, J. (2009). Amphotericin B and its new derivatives – mode of action. Curr. Drug Metab. *10*, 459–469.

Barger, S.R., Hoefler, B.C., Cubillos-Ruiz, A., Russell, W.K., Russell, D.H., and Straight, P.D. (2012). Imaging secondary metabolism of *Streptomyces* sp. Mg1 during cellular lysis and colony degradation of competing *Bacillus subtilis*. Antonie Van Leeuwenhoek *102*, 435–445.

Berleman, J.E., Allen, S., Danielewicz, M.A., Remis, J.P., Gorur, A., Cunha, J., Hadi, M.Z., Zusman, D.R., Northen, T.R., Witkowska, H.E., et al. (2014). The lethal cargo of *Myxococcus xanthus* outer membrane vesicles. Front. Microbiol. *5*, 474.

Blodgett, J.A.V., Zhang, J.K., and Metcalf, W.W. (2005). Molecular cloning, sequence analysis, and heterologous expression of the phosphinothricin tripeptide biosynthetic gene cluster from *Streptomyces viridochromogenes* DSM 40736. Antimicrob. Agents Chemother. *49*, 230–240.

Borić, M., Danevčič, T., and Stopar, D. (2011). Prodigiosin from *Vibrio* sp. DSM 14379; a new UV-protective pigment. Microb. Ecol. *62*, 528–536.

Branda, S.S., Gonzalez-Pastor, J.E., Ben-Yehuda, S., Losick, R., and Kolter, R. (2001). Fruiting body formation by *Bacillus subtilis*. Proc. Natl. Acad. Sci. USA *98*, 11621–11626.

Brown, L., Kessler, A., Cabezas-Sanchez, P., Luque-Garcia, J.L., and Casadevall, A. (2014). Extracellular vesicles produced by the Gram-positive bacterium *Bacillus subtilis* are disrupted by the lipopeptide surfactin. Mol. Microbiol. *93*, 183–198.

Brown, L., Wolf, J.M., Prados-Rosales, R., and Casadevall, A. (2015). Through the wall: extracellular vesicles in Gram-positive bacteria, mycobacteria and fungi. Nat. Rev. Microbiol. *13*, 620–630.

Cai, P., Kong, F., Fink, P., Ruppen, M.E., Williamson, R.T., and Keiko, T. (2007). Polyene antibiotics from *Streptomyces mediocidicus*. J. Nat. Prod. *70*, 215–219.

Caiazza, N.C., Shanks, R.M.Q., and O'Toole, G.A. (2005). Rhamnolipids modulate swarming motility patterns of *Pseudomonas aeruginosa*. J. Bacteriol. *187*, 7351–7361.

Challis, G.L., and Hopwood, D.A. (2003). Synergy and contingency as driving forces for the evolution of multiple secondary metabolite production by *Streptomyces* species. Proc. Natl. Acad. Sci. USA *100*, 14555–14561.

Cortés-Sánchez Ade, J., Hernández-Sánchez, H., and Jaramillo-Flores, M.E. (2013). Biological activity of glycolipids produced by microorganisms: new trends and possible therapeutic alternatives. Microbiol. Res. *168*, 22–32.

Gay, D., You, Y.-O., Keatinge-Clay, A., and Cane, D.E. (2013). Structure and stereospecificity of the dehydratase domain from the terminal module of the rifamycin polyketide synthase. Biochemistry *52*, 8916–8928.

Gerber, N.N. (1975). A new prodiginine (prodigiosin-like) pigment from Streptomyces. antimalarial activity of several prodiginines. J. Antibiot. (Tokyo) *28*, 194–199.

Gouy, M., Guindon, S., and Gascuel, O. (2010). SeaView version 4: a multiplatform graphical user interface for sequence alignment and phylogenetic tree building. Mol. Biol. Evol. *27*, 221–224.

Gust, B., Challis, G.L., Fowler, K., Kieser, T., and Chater, K.F. (2003). PCR-targeted *Streptomyces* gene replacement identifies a protein domain needed for biosynthesis of the sesquiterpene soil odor geosmin. Proc. Natl. Acad. Sci. USA *100*, 1541–1546.

Gust, B., Chandra, G., Jakimowicz, D., Yuqing, T., Bruton, C.J., and Chater, K.F. (2004). λ red-mediated genetic manipulation of antibiotic-producing *Streptomyces*. Adv. Appl. Microbiol. *54*, 107–128.

Hider, R.C., and Kong, X. (2010). Chemistry and biology of siderophores. Nat. Prod. Rep. *27*, 637–657.

Hoefler, B.C., Gorzelnik, K.V., Yang, J.Y., Hendricks, N., Dorrestein, P.C., and Straight, P.D. (2012). Enzymatic resistance to the lipopeptide surfactin as identified through imaging mass spectrometry of bacterial competition. Proc. Natl. Acad. Sci. USA *109*, 13082–13087.

Hoefler, B.C., Konganti, K., and Straight, P.D. (2013). De novo assembly of the *Streptomyces* sp. strain Mg1 genome using PacBio single-molecule sequencing. Genome Announc. *1*, http://dx.doi.org/10.1128/genomeA.00535-13.

Hong, H., Fill, T., and Leadlay, P.F. (2013). A common origin for guanidinobutanoate starter units in antifungal natural products. Angew. Chem. *125*, 13334–13337.

Igarashi, Y., Iwashita, T., Fujita, T., Naoki, H., Yamakawa, T., Yoshida, R., and Furumai, T. (2003). Clethramycin, a new inhibitor of pollen tube growth with antifungal activity from *Streptomyces hygroscopicus* TP-A0623 II. Physicochemical properties and structure determination. J. Antibiot. (Tokyo) *56*, 705–708.

Kearns, D.B., and Losick, R. (2004). Swarming motility in undomesticated *Bacillus subtilis*. Mol. Microbiol. *49*, 581–590.

Keatinge-Clay, A. (2008). Crystal structure of the erythromycin polyketide synthase dehydratase. J. Mol. Biol. *384*, 941–953.

Keatinge-Clay, A.T. (2007). A tylosin ketoreductase reveals how chirality is determined in polyketides. Chem. Biol. *14*, 898–908.

Keatinge-Clay, A.T., and Stroud, R.M. (2006). The structure of a ketoreductase determines the organization of the β-carbon processing enzymes of modular polyketide synthases. Structure *14*, 737–748.

Kinsinger, R.F., Shirk, M.C., and Fall, R. (2003). Rapid surface motility in *Bacillus subtilis* is dependent on extracellular surfactin and potassium ion. J. Bacteriol. *185*, 5627–5631.

Kulp, A., and Kuehn, M.J. (2010). Biological functions and biogenesis of secreted bacterial outer membrane vesicles. Annu. Rev. Microbiol. *64*, 163–184.

Kwan, D.H., and Schulz, F. (2011). The stereochemistry of complex polyketide biosynthesis by modular polyketide synthases. Molecules *16*, 6092–6115.

Lee, E.-Y., Choi, D.-Y., Kim, D.-K., Kim, J.-W., Park, J.O., Kim, S., Kim, S.-H., Desiderio, D.M., Kim, Y.-K., Kim, K.-P., et al. (2009). Gram-positive bacteria produce membrane vesicles: proteomics-based characterization of *Staphylococcus aureus*-derived membrane vesicles. Proteomics *9*, 5425–5436.

Lee, J.H., Choi, C.-W., Lee, T., Kim, S., Lee, J.-C., Shin, J.-H., Wiedmann, M., Arvik, T., Hurley, R., Boor, K., et al. (2013). Transcription factor σB plays an important role in the production of extracellular membrane-derived vesicles in *Listeria monocytogenes*. PLoS One *8*, e73196.

López, D., Fischbach, M.A., Chu, F., Losick, R., and Kolter, R. (2009). Structurally diverse natural products that cause potassium leakage trigger multicellularity in *Bacillus subtilis*. Proc. Natl. Acad. Sci. USA *106*, 280–285.

Manteca, A., Alvarez, R., Salazar, N., Yagüe, P., and Sanchez, J. (2008). Mycelium differentiation and antibiotic production in submerged cultures of *Streptomyces coelicolor*. Appl. Environ. Microbiol. *74*, 3877–3886.

Martínez-Castro, M., Solera, E., Martín, J.F., and Barreiro, C. (2009). Efficient pyramidal arrangement of an ordered cosmid library: rapid screening of genes of the tacrolimus-producer *Streptomyces* sp. ATCC 55098. J. Microbiol. Methods *78*, 150–154.

Mashburn, L.M., and Whiteley, M. (2005). Membrane vesicles traffic signals and facilitate group activities in a prokaryote. Nature *437*, 422–425.

Mashburn-Warren, L., Howe, J., Brandenburg, K., and Whiteley, M. (2009). Structural requirements of the *Pseudomonas quinolone* signal for membrane vesicle stimulation. J. Bacteriol. *191*, 3411–3414.

McAlpine, J.B., Bachmann, B.O., Piraee, M., Tremblay, S., Alarco, A.-M., Zazopoulos, E., and Farnet, C.M. (2005). Microbial genomics as a guide to drug discovery and structural elucidation: ECO-02301, a novel antifungal agent, as an example. J. Nat. Prod. *68*, 493–496.

Meschke, H., Walter, S., and Schrempf, H. (2012). Characterization and localization of prodiginines from *Streptomyces lividans* suppressing *Verticillium dahliae* in the absence or presence of *Arabidopsis thaliana*. Environ. Microbiol. *14*, 940–952.

Miyaoka, R., Hosokawa, M., Ando, M., Mori, T., Hamaguchi, H., and Takeyama, H. (2014). In situ detection of antibiotic amphotericin B produced in *Streptomyces nodosus* using Raman microspectroscopy. Mar. Drugs *12*, 2827–2839.

Nguyen, D.D., Wu, C.-H., Moree, W.J., Lamsa, A., Medema, M.H., Zhao, X., Gavilan, R.G., Aparicio, M., Atencio, L., Jackson, C., et al. (2013). MS/MS networking guided analysis of molecule and gene cluster families. Proc. Natl. Acad. Sci. USA *110*, E2611–E2620.

Ostash, B., Saghatelian, A., and Walker, S. (2007). A streamlined metabolic pathway for the biosynthesis of moenomycin A. Chem. Biol. *14*, 257–267.

Petković, H., Sandmann, A., Challis, I.R., Hecht, H.-J., Silakowski, B., Low, L., Beeston, N., Kuščer, E., Garcia-Bernardo, J., Leadlay, P.F., et al. (2008). Substrate specificity of the acyl transferase domains of EpoC from the epothilone polyketide synthase. Org. Biomol. Chem. *6*, 500–506.

Prados-Rosales, R., Baena, A., Martinez, L.R., Luque-Garcia, J., Kalscheuer, R., Veeraraghavan, U., Camara, C., Nosanchuk, J.D., Besra, G.S., Chen, B., et al. (2011). Mycobacteria release active membrane vesicles that modulate immune responses in a TLR2-dependent manner in mice. J. Clin. Invest. *121*, 1471–1483.

Raguso, R.A., Agrawal, A.A., Douglas, A.E., Jander, G., Kessler, A., Poveda, K., and Thaler, J.S. (2015). The raison d'être of chemical ecology. Ecology *96*, 617–630.

R Core Team. (2013). R: A Language and Environment for Statistical Computing (R Foundation for Statistical Computing). http//www.r-project.org.

Ruijter, J.M., Ramakers, C., Hoogaars, W.M.H., Karlen, Y., Bakker, O., Van Den Hoff, M.J.B., and Moorman, A.F.M. (2009). Amplification efficiency: linking baseline and bias in the analysis of quantitative PCR data. Nucleic Acids Res. *37*, e45.

Sakuda, S., Guce-Bigol, U., Itoh, M., Nishimura, T., and Yamada, Y. (1995). Linearmycin A, a novel linear polyene antibiotic. Tetrahedron Lett. *36*, 2777–2780.

Sakuda, S., Guce-Bigol, U., Itoh, M., Nishimura, T., and Yamada, Y. (1996). Novel linear polyene antibiotics: linearmycins. J. Chem. Soc. Perkin Trans. 1 *36*, 2315.

Sato, T., Konno, H., Tanaka, Y., Kataoka, T., Nagai, K., Wasserman, H.H., and Ohkuma, S. (1998). Prodigiosins as a new group of H+/Cl-symporters that uncouple proton translocators. J. Biol. Chem. *273*, 21455–21462.

Schertzer, J.W., and Whiteley, M. (2012). A bilayer-couple model of bacterial outer membrane vesicle biogenesis. MBio *3*, http://dx.doi.org/10.1128/mBio.00297-11.

Schneider, C.A., Rasband, W.S., and Eliceiri, K.W. (2012). NIH Image to ImageJ: 25 years of image analysis. Nat. Methods *9*, 671–675.

Schrempf, H., and Merling, P. (2015). Extracellular *Streptomyces lividans* vesicles: composition, biogenesis and antimicrobial activity. Microb. Biotechnol. *8*, 644–658.

Schrempf, H., Koebsch, I., Walter, S., Engelhardt, H., and Meschke, H. (2011). Extracellular *Streptomyces* vesicles: amphorae for survival and defence. Microb. Biotechnol. *4*, 286–299.

Schwechheimer, C., and Kuehn, M.J. (2015). Outer-membrane vesicles from Gram-negative bacteria: biogenesis and functions. Nat. Rev. Microbiol. *13*, 605–619.

Shannon, P., Markiel, A., Ozier, O., Baliga, N.S., Wang, J.T., Ramage, D., Amin, N., Schwikowski, B., and Ideker, T. (2003). Cytoscape: a software environment for integrated models of biomolecular interaction networks. Genome Res. *13*, 2498–2504.

Sievers, F., and Higgins, D.G. (2014). Clustal omega, accurate alignment of very large numbers of sequences. Methods Mol. Biol. *1079*, 105–116.

Stankovic, N., Radulovic, V., Petkovic, M., Vuckovic, I., Jadranin, M., Vasiljevic, B., and Nikodinovic-Runic, J. (2012). *Streptomyces* sp. JS520 produces exceptionally high quantities of undecylprodigiosin with antibacterial, antioxidative, and UV-protective properties. Appl. Microbiol. Biotechnol. *96*, 1217–1231.

Strohalm, M., Hassman, M., Košata, B., and Kodíček, M. (2008). mMass data miner: an open source alternative for mass spectrometric data analysis. Rapid Commun. Mass. Spectrom. *22*, 905–908.

Stubbendieck, R.M., and Straight, P.D. (2015). Escape from lethal bacterial competition through coupled activation of antibiotic resistance and a mobilized subpopulation. PLoS Genet. *11*, e1005722.

Stubbendieck, R.M., Vargas-Bautista, C., and Straight, P.D. (2016). Bacterial communities: interactions to scale. Front. Microbiol. *7*, 1234.

Traxler, M.F., and Kolter, R. (2015). Natural products in soil microbe interactions and evolution. Nat. Prod. Rep. *32*, 956–970.

Tsao, S.-W., Rudd, B.A.M., He, X.-G., Chang, C.-J., and Floss, H.G. (1985). Identification of a red pigment from *Streptomyces coelicolor* A3(2) as a mixture of prodigiosin derivatives. J. Antibiot. (Tokyo) *38*, 128–131.

Turnbull, L., Toyofuku, M., Hynen, A.L., Kurosawa, M., Pessi, G., Petty, N.K., Osvath, S.R., Cárcamo-Oyarce, G., Gloag, E.S., Shimoni, R., et al. (2016). Explosive cell lysis as a mechanism for the biogenesis of bacterial membrane vesicles and biofilms. Nat. Commun. *7*, 11220.

Upadhyay, S., Xu, X., Lowry, D., Jackson, J.C., Roberson, R.W., and Lin, X. (2016). Subcellular compartmentalization and trafficking of the biosynthetic machinery for fungal melanin. Cell Rep. *14*, 2511–2518.

Uttlová, P., Pinkas, D., Bechyňková, O., Fišer, R., Svobodová, J., and Seydlová, G. (2016). *Bacillus subtilis* alters the proportion of major membrane phospholipids in response to surfactin exposure. Biochim. Biophys. Acta Biomembr. *1858*, 2965–2971.

Valenzano, C.R., You, Y.-O., Garg, A., Keatinge-Clay, A., Khosla, C., and Cane, D.E. (2010). Stereospecificity of the dehydratase domain of the erythromycin polyketide synthase. J. Am. Chem. Soc. *132*, 14697–14699.

Waterhouse, A.M., Procter, J.B., Martin, D.M.A., Clamp, M., and Barton, G.J. (2009). Jalview version 2 – a multiple sequence alignment editor and analysis workbench. Bioinformatics *25*, 1189–1191.

Waters, C.M., and Bassler, B.L. (2005). Quorum sensing: cell-to-cell communication in bacteria. Annu. Rev. Cell Dev. Biol. *21*, 319–346.

Watrous, J., Roach, P., Alexandrov, T., Heath, B.S., Yang, J.Y., Kersten, R.D., van der Voort, M., Pogliano, K., Gross, H., Raaijmakers, J.M., et al. (2012). Mass spectral molecular networking of living microbial colonies. Proc. Natl. Acad. Sci. USA *109*, E1743–E1752.

Wickham, H. (2009). ggplot2: Elegant Graphics for Data Analysis (Springer).

Williams, R.P., Green, J.A., Rappoport, D.A., Green, J.A., Rappoport, D.A., and Wein-Berg, E.D. (1956). Studies on pigmentation of *Serratia marcescens* I: spectral and paper chromatographic properties of prodigiosin. J. Bacteriol. *71*, 115–120.

Xue, Y., and Sherman, D.H. (2000). Alternative modular polyketide synthase expression controls macrolactone structure. Nature *403*, 571–575.

Zhao, Y., Xiang, S., Dai, X., and Yang, K. (2013). A simplified diphenylamine colorimetric method for growth quantification. Appl. Microbiol. Biotechnol. *97*, 5069–5077.

Zheng, J., Piasecki, S.K., and Keatinge-Clay, A.T. (2013). Structural studies of an A2-type modular polyketide synthase ketoreductase reveal features controlling α-substituent stereochemistry. ACS Chem. Biol. *8*, 1964–1971.

STAR★METHODS

KEY RESOURCES TABLE

REAGENT or RESOURCE	SOURCE	IDENTIFIER
Bacterial and Virus Strains		
See Table S1 for Bacterial Strain Table		
Oligonucleotides		
See Table S2 for Primer Table		
Software and Algorithms		
Clustal Omega	Sievers and Higgins, 2014	http://www.clustal.org/omega/
Cytoscape	Shannon et al., 2003	http://www.cytoscape.org/
Global Natural Product Social Molecular Networking	Watrous et al., 2012; Nguyen et al., 2013	http://gnps.ucsd.edu
ImageJ	Schneider et al., 2012	https://imagej.nih.gov/ij/
Jalview	Waterhouse et al., 2009	http://www.jalview.org/
LinReg	Ruijter et al., 2009	http://www.hartfaalcentrum.nl/index.php?main=files&sub=LinRegPCR
mMass	Strohalm et al., 2008	http://www.mmass.org/
SBSPKS	Anand et al., 2010	www.nii.ac.in/sbspks.html
Xcalibur		https://www.thermofisher.com/order/catalog/product/OPTON-30487

CONTACT FOR REAGENT AND RESOURCE SHARING

Further information and requests for resources and reagents should be directed to and will be fulfilled by the lead contact, Paul D. Straight (paul_straight@tamu.edu).

EXPERIMENTAL MODEL AND SUBJECT DETAILS

Bacterial Strains, Primers, and Media

Bacterial strains and primers used in this study are listed in Table S1 and Table S2, respectively. Common salts, buffers, and other reagents were purchased from Sigma-Aldrich, Amresco, or Mallinckrodt. Amino acids were purchased from Sigma-Aldrich. Solvents were HPLC grade and purchased from Macron. *Bacillus subtilis* and *Escherichia coli* overnight cultures were prepared in LB [1% w/v tryptone, 0.5% yeast extract, and 0.5% NaCl]. Spore suspensions of *Streptomyecs* sp. Mg1 (*S.* Mg1) were prepared using standard procedures. *Streptomyces* cultures and co-cultures were prepared on Maltose-Yeast Extract-Malt Extract (MYM) [0.4% w/v malt extract, 0.4% yeast extract, 0.4% D-(+)-maltose monohydrate (Sigma), and 1.5% w/v agar], or Glucose-Yeast Extract-Malt Extract (GYM) [1% w/v malt extract, 0.4% yeast extract, 0.4% D-(+)-glucose (BDH), and 1.5% w/v agar]. Where indicated, MYM or GYM media was buffered [100 mM MOPS (Chem-Impex) and 5 mM potassium phosphate at pH 7]. Buffered MYM media prepared without agar was used for growth of *S.* Mg1 in liquid culture. AS1 plates [0.1% w/v yeast extract, 0.02% L-alanine, 0.02% L-arginine free base, 0.05% L-asparagine, 0.5% soluble starch (Difco), 0.25% NaCl, 1% Na_2SO_4, 10 mM $MgCl_2$, and 1.5% agar] were used for conjugations.

METHOD DETAILS

Extraction and Purification of Linearmycins

Buffered MYM media without agar (4 × 1 L in 4 L Erlenmeyer flasks) was inoculated with 10^6 spores/ml of *S.* Mg1 from a freshly prepared spore suspension. The cultures were incubated at 30°C in the dark on a shaking platform with 1 inch throw at 250 rpm for 7 days. All linearmycin extraction and purification procedures were carried out in the dark as described previously (Stubbendieck and Straight, 2015). The *S.* Mg1 mycelial mats were collected by filtration on Whatman #3 qualitative circles. The combined mycelial mass was extracted sequentially with 500 ml methanol (MeOH) and 500 ml ethanol (EtOH) (25°C, 30 min, shaking at 200 rpm). The extracts were combined and concentrated to 100 ml under reduced pressure. Diaion HP-20 resin (20 g, wetted in MeOH) was added, and the extract was evaporated to dryness. The adsorbed resin was resuspended in 20 ml MeOH, the flask was swirled a few times to ensure complete wetting, and 180 ml 20 mM ammonium bicarbonate (NH_4HCO_3) pH 10 was added. Meanwhile, the culture supernatants were combined, adjusted to pH 10 with ammonium hydroxide, and 450 ml MeOH was added. Diaion HP-20 resin

(20 g, wetted in MeOH, equilibrated in 10% MeOH/20 mM NH_4HCO_3 pH 10) was added to the treated supernatants. The suspension was stirred gently (100 rpm) at ambient temperature for 30 minutes. A fritted glass column (40 mm x 300 mm, medium frit) was packed with Diaion HP-20 resin (20 g, wetted in MeOH, equilibrated in 10% MeOH/20 mM NH_4HCO_3 pH 10). The mycelial extraction suspension was poured over the column. The resin from the suspension was collected on the top of the column and the flowthrough was discarded. The column was washed stepwise with EtOH/20 mM NH_4HCO_3 pH 10 (100 ml 10% EtOH followed by 200 ml each 20%, 40%, and 50% EtOH). The washes were discarded and the column was eluted twice with 200 ml 100% EtOH. The eluates were combined and evaporated to dryness.

The extract residue was redissolved in a small volume of EtOH and concentrated to ∼5 ml under reduced pressure. Insoluble precipitates were removed by centrifugation. The soluble fraction was filtered, stabilized by addition of 50 ppm BHT, and chromatographed on an Agilent 1200 HPLC equipped with an autosampler, quaternary pump, thermostatted column compartment, UV-Vis DAD detector, and fraction collector. A semipreparative (10 x 250 mm, 5 μm) Phenomenex Luna C18 column with a guard column (10 x 10 mm, 3 μm) was equilibrated with 64% 20 mM NH_4HCO_3 pH 7 (solvent A), 28% ACN (solvent B), 8% MeOH (solvent C) flowing at 5 ml/min with the temperature held at 30°C. All solvents were degassed and sparged with nitrogen prior to HPLC. The extract was injected (100 μl) repeatedly onto the column and eluted with a gradient program: 1) wash postinjection 64:28:8% (solvent A:B:C) 2 min, 2) ramp to 58:34:8% over 1 min, 3) hold at 58:34:8% 5 min, 4) ramp to 52:38:10% over 10 min, 5) hold at 52:38:10% for 10 min, 6) ramp to 64:28:8% over 2 min, 7) reequilibrate with 64:28:8% for 5 min. Fraction collection was triggered by minimum threshold absorbance at 333 nm above the baseline. Linearmycin A co-eluted with a carbohydrate-containing impurity in the 17-18 min time window. Linearmycins B and C co-eluted as a single peak in the 24-26 min time window. For further purification of linearmycin A, the fractions containing linearmycin A were pooled, concentrated, and re-chromatographed using a second gradient program: 1) wash postinjection 64:28:8% (solvent A:B:C) 2 min, 2) ramp to 55:35:10% over 10 min, 3) hold at 55:35:10% 13 min, 4) ramp to 64:28:8% over 2 min, 5) reequilibrate with 64:28:8% for 3 min. Fractions containing linearmycin A were collected in the 21-23 min time window and pooled. The fractions were sequentially evaporated, redissolved in 20% EtOH/water, evaporated, redissolved in 20% EtOH/water, partially concentrated, and lyophilized to remove the NH_4HCO_3 buffer, yielding pure linearmycin A (typically 1-3 mg): ESI-MS m/z 1140.7229 $[M^+H]^+$ ($C_{64}H_{102}NO_{16}$ requires 1140.7193, error = 3.2 ppm), λ_{max}(MeOH)(ε) 319 (30,000), 332 (32,000), 351 (25,000). To separate linearmycins B and C, the pooled fractions containing them were re-chromatographed using a HILIC method. An analytical (4.6 x 200 mm, 5 μm, 200 Å) PolyLC polyhydroxyethyl column was equilibrated with 18% 20 mM NH_4HCO_3 pH 7 (solvent A), 82% ACN (solvent B) flowing at 1.5 ml/min with the temperature held at 35°C. The fractions were concentrated, injected repeatedly (20 μl), and eluted isocratically. Fractions with UV absorbance at 333 nm were collected in the 16-18 min (linearmycin C) and 18-20 min (linearmycin B) time windows. Conservative fraction pooling and removal of the NH_4HCO_3 buffer as described for linearmycin A yielded pure linearmycin B and C (typically 1-2 mg of each): ESI-MS m/z 1166.7385 $[M^+H]^+$ ($C_{66}H_{104}NO_{16}$) requires 1166.7350, error = 3.0 ppm), λ_{max}(MeOH)(ε) 319 (96,000), 334 (144,000), 351 (104 000); ESI-MS m/z 1180.7539 $[M^+H]^+$ ($C_{67}H_{106}NO_{16}$) requires 1180.7506, error = 2.8 ppm), λmax (MeOH)(ε) 319 (76,000), 334 (114 000), 351 (82,000).

Accurate Linearmycin Mass Determination

An analytical (2.1 x 150 mm, 3 μm, 120 Å) Thermo Scientific Acclaim 120 C18 column attached to a Thermo Scientific Orbitrap Exactive LC-MS was equilibrated with 65% water/0.1% formic acid (solvent A), 35% 1:1 ACN:IPA (solvent B) flowing at 0.25 ml/min. Purified linearmycin samples were diluted to ∼10 μg/ml in MeOH, injected (50 μl), and eluted with a gradient program: 1) wash post-injection 65:35% (solvent A:B) 2 min, 2) ramp to 58:42% over 1 minute, 3) hold at 58:42% 5 min, 4) ramp to 52:48% over 7 min, 5) hold at 52:48% for 5 mins, 6) ramp to 20:80% over 5 min, 7) ramp to 65:35% over 5 min, 8) reequilibrate with 65:35% for 5 min. Mass spec acquisition parameters: positive mode, mass range m/z 1041-1291, HESI source (spray voltage: 4800 V, capillary temp: 250°C, sheath gas: 40, aux gas: 20, max spray current: 100 μA, heater temp: 200°C), Orbitrap mass analyzer (extraction time: 1 Hz, AGC target: 5×10^5, injection time: 50 ms, 1 microscan per scan, calibrated with LTQ ESI positive and negative ion calibration solutions from Pierce), tune settings (capillary: 77.50 V, tube lens: 185 V, skimmer: 46 V, RF0 DC offset: 12 V, lens 1: 0 V, MP0 and MP1 RF: 700 V, RF1 DC offset: 7 V, MP2 and MP3 RF: 700 V, gate lens: 6.75 V, c-trap RF: 2400 V). A 1 μg/ml sample of ECO-02301 dissolved in MeOH was flowed in post-column for use as a lock mass. Spectra were averaged, exported to mzXML, and processed using mMass (http://www.mmass.org/) (Strohalm et al., 2008). Accurate mass determinations were made and used for molecular formula predictions.

MS/MS of Linearmycins

To collect MS/MS spectra of linearmycins, the LC method for accurate mass determination was used with the following modifications to the mass spec acquisition parameters: Orbitrap mass analyzer (AGC target: 1×10^6, no lock mass), scan 1 (positive mode, mass range m/z 800-1400, extraction time: 2 Hz), scan 2 (positive mode, mass range: m/z 200-1400, extraction time: 4 Hz, collision cell: HCD 50 eV). MS/MS spectra were selected, exported to mzXML, and processed using mMass.

UV-Vis Measurements of Linearmycins

HPLC purified and lyophilized samples of linearmycins were accurately weighed and redissolved to a standardized concentration of 2 mg/ml in MeOH. For UV-Vis spectrum measurements, linearmycins were diluted 1:200 (5 μl into 995 μl MeOH) and placed in a

quartz cuvette (Hellma, 1 cm path length). The UV-Vis spectrum was measured by a wavelength scan (210-450 nm, 120 nm/min) after blanking on a Beckman DU-650 spectrophotemeter. Data files were exported in ASCII format and spectra were plotted using the Gnumeric spreadsheet software.

NMR Analysis of Linearmycins

1D and 2D NMR measurements in MeOH-d_4 were collected on Bruker Avance 500, 600, and 800 MHz instruments equipped with triple resonance (H-C-N) cryoprobes. Experiments acquired included 1D ^{1}H (500, 600, 800) and ^{13}C (800), COSY (500, 800), HSQC (500, 800), TOCSY (500), HSQC-TOCSY (500), ROESY (500, 800), H2BC (600), and HMBC (600). Chemical shifts are reported in Table S4. The following basic strategy was used for structural assignment of linearmycin C. Examination of the 1D ^{13}C and HSQC spectra defined the carbon inventory the molecule: 1 ketone, 1 carboxylic acid, 28 olefins, 13 carbinols, 17 methylenes, 3 methines, and 4 methyl groups. This is consistent with the molecular formula $C_{67}H_{105}NO_{16}$ determined from the accurate mass (Figure S1C). Stepwise analysis of COSY, HSQC, TOCSY, and HSQC-TOCSY correlations defined the major fragments of the molecule: a polyene terminating in a carboxylic acid, a second polyene, two 1,3-butanediol groups, a carbinol flanked by two olefins, a four carbinol tetra-hydroxyl fragment flanked by two olefins, and a three carbinol tri-hydroxyl fragment flanked by one olefin and the ketone. Complete assignment in the case of overlapping peaks was assisted by the H2BC spectrum. Quaternary carbons and methyl groups were placed by COSY, H2BC, and HMBC. The polyenes were defined as two pentaenes by analysis of the UV-Vis spectrum (Figure S1C) and assigned using a combination of COSY, H2BC, and a series of 1D selective COSY and TOCSY experiments. Finally, the fragments were linked together by COSY, HSQC, H2BC, and HMBC correlations into a linear structure. The starter unit was defined as a δ-aminobutyl structure by HSQC-TOCSY, and the linear topology of the molecule was confirmed by ROESY. For confirmation of the linearmycin B structure, the HSQC spectrum of linearmycin B was superimposed with the HSQC of linearmycin C. The primary difference identified for linearmycin B was a missing methylene in the starter unit, making it a γ-aminopropyl structure. For confirmation of the linearmycin A structure, the HSQC of linearmycin A was superimposed with the HSQC of linearmycin B. The primary difference identified for linearmycin A was a missing olefin in the terminal pentaene attached to the carboxylic acid. The linearmycin A and B structures match the published data (Sakuda et al., 1995, 1996; Stubbendieck and Straight, 2015), and the backbone for all three linearmycin structures is consistent with the predicted structure obtained from bioinformatic analysis of the biosynthetic gene cluster.

Linearmycin Gene Cluster Analysis

To identify the linearmycin gene cluster in *S.* Mg1, the genomic sequence (GenBank: CP011664.1) (Hoefler et al., 2013) was scanned for predicted modular polyketide synthases (PKSs). A large cluster consisting of nine PKS open-reading frames was identified near the left arm of the chromosome. Domain prediction of the PKSs was carried out using SBSPKS (Anand et al., 2010). Identified acyl-transferase, ketoreductase, and dehydratase domains were aligned with Clustal Omega (Sievers and Higgins, 2014) and annotated with Jalview (Waterhouse et al., 2009). Functional analysis of the domains was based on published X-ray crystallography data. Acyltransferases were identified as malonyl-CoA type or methylmalonyl-CoA type by the presence of conserved HAFH or YASH motifs (Petković et al., 2008), respectively, in the active site. The inactive ketoreductase of *InyHD* was identified by a mutation of the conserved catalytic tyrosine to a glutamine. Of the remaining active ketoreductases most were predicted to be A-type ((D)-hydroxy-yacyl-forming), but two ketoreductases in *InyHA* and *InyHB* were predicted to be B-type ((L)-hydroxyacyl-forming) by mutations in the conserved LDD active-site motif accompanied by a downstream tryptophan active-site residue (Keatinge-Clay, 2007; Keatinge-Clay and Stroud, 2006; Kwan and Schulz, 2011; Zheng et al., 2013). For the dehydratase analysis, only the first 170-180 amino acid residues of each dehydratase domain were identified by SBSPKS leaving critical active-site residues absent. To work around this, alignments were carried out using the predicted dehydratase sequence along with the downstream inter-domain "linker region" sequence. Mutations in the GYXYGPXF, DXXXQ/H, and LPFXW consensus active-site motifs identified two likely inactive dehydratase domains in *InyHB* and *InyHC*. All of the predicted active dehydratases neighbor A-type ketoreductases, indicating that all olefins in the molecule likely have an E (or "*trans*") configuration (Gay et al., 2013; Keatinge-Clay, 2008; Kwan and Schulz, 2011; Valenzano et al., 2010). For thioesterase analysis, the thioesterase sequence was aligned with known thioesterases from macrolides (ex: erythromycin), macrolide polyenes (ex: nystatin), and linear polyenes (ex: ECO-02301). Sequence similarity was visualized by construction of a phylogenetic tree using Seaview (Gouy et al., 2010). For biosynthesis of the starter unit, predicted open-reading frames flanking the PKS genes were analyzed. A predicted agamatinase (*InyT*), amine oxidase (*InyO*), acyl-CoA ligase (*InyN*), and ACP S-malonyl acyltransferase (*InyI*) were identified, allowing for a proposed biosynthesis of an aminoalkyl starter unit originating from arginine. All of the bioinformatic analysis taken together allows for prediction of a linear molecule consistent with the published structure for linearmycin B. The linearmycin A variant must arise from "module-skipping" within *InyHH* or *InyHI* prior to incorporation and hydrolysis of the final methylmalonyl-CoA. The linearmycin C variant must arise from incorporation of an additional methylene into the starter unit.

Cosmid Library Preparation and *Iny* Gene Cluster Identification

Disruption of linearmycin biosynthesis in *S.* Mg1 was achieved by deletion of the *InyI* acyltransferase using the REDIRECT procedure (Gust et al., 2004; Martínez-Castro et al., 2009). Genomic DNA from *S.* Mg1 was manually sheared by passing it through a Hamilton syringe needle. The sheared DNA was end-repaired and size-selected by pulsed-field gel electrophoresis (1% agarose in 0.5X TBE, 15 h at 14°C, 6 V/cm, 5-8 second switch time linear ramp, 120° switch angle) on a CHEF (Bio-Rad) apparatus. A 40 kb cosmid control

and lambda phage DNA concatemers were used as size markers in neighboring lanes. The gel was stained with SYBR (Invitrogen) and a gel slice migrating near the 40 kb marker bands was excised. The DNA was recovered from the gel slice and ligated into the pWEB cosmid vector (Epicentre). The ligated cosmid DNA was packaged into lambda phage heads (Epicentre), and the phages were used to infect *E. coli* EC100 host cells. The cells were plated on selective media and 1500 clones, representing ~3x coverage of the genome, were individually frozen in 96-well plates at -80°C in 20% glycerol. Cosmid pool plates were additionally constructed to facilitate screening. The 16 96-well plates of the library were used to construct 4 96-well plate pooled libraries (4 clones/well) by growing individual clones in selective media to the same OD_{600} and mixing 50 μl of each of 4 clones from corresponding wells of different library plates to make 200 μl pooled wells in the pooled plates (ex: wells A1 from library plates 1-4 were pooled to well A1 of pooled plate 1). A similar procedure was used to construct a single master pool plate containing the whole cosmid library (16 clones/well).

The *S.* Mg1 cosmid library was screened for cosmids overlapping the linearmycin gene cluster in a hierarchical fashion by real-time PCR. Primers SM066 and SM067 were designed to amplify a 350 bp product from the left-flanking genomic region of the linearmycin gene cluster. Cells from the master pool plate were lysed by the alkaline lysis method, and the crude lysates were used as templates for real-time PCR. Wells yielding positive amplification reactions were used to identify corresponding wells in the quaternary pools, which were screened again by real-time PCR. Positive amplifications reactions from this secondary screen were used to pick individual clones from the library for a final screening by real-time PCR. Screening in this fashion was efficient and could be used to quickly identify overlapping cosmids within two days. Cosmids in clones identified by real-time PCR were purified (Sigma PhasePrep) and end-sequenced to determine the precise genomic coordinates of the insert. One identified cosmid (15B10) with the target *lnyI* gene near the middle of the insert was used for further manipulations. The the *lnyI* gene was amplified with 400 bp of the 5' UTR using primers EMH029 and EMH030 and cloned into the pOOB407 *attB*-integrating vector (Ostash et al., 2007) for subsequent work.

Mutagenesis of *lnyI* and Genetic Complementation

The 15B10 cosmid was transformed into *E. coli* BW25113 harboring the λ-RED plasmid pIJ790. Primers SM080 and SM081 were used to target the *lnyI* gene for in-frame replacement with an apramycin resistance cassette. Mutated cosmid selected on apramycin was transferred to *S.* Mg1 by conjugation with the *E. coli* WM3780 methylation-deficient donor strain using published methods (Blodgett et al., 2005; Gust et al., 2003, 2004). Exconjugants were passaged once with nalidixic acid (30 μg/ml) and apramycin (50 μg/ml) selection, sporulated without antibiotics present, and spore stock dilutions were plated on apramycin-containing plates. Single apramycin-resistant colonies were picked and allelic replacement of *lnyI* was confirmed by PCR.

The complement strain was generated by PCR amplification of the native *lnyI* gene with 400 bp of the 5' UTR using primers EMH029 and EMH030. The PCR product was cloned into the pOOB407 *attB*-integrating vector (Ostash et al., 2007) and transferred to the *S.* Mg1 Δ*lnyI* strain by conjugation. Complementation was confirmed by PCR using primers BCH166 and BCH167. Exconjugantes were selected and passaged on media containing apramycin and hygromycin (50 μg/ml).

Co-culture Plates

Co-culture experiments were generally carried out as described previously (Barger et al., 2012). *Streptomyces sp.* Mg1 wild type and mutant strains were plated as lawns at a spore density of 10^5 spores per 100 mm plate on buffered GYM media. The plates were dried in a laminar flow hood for 20–30 min before plating. A 2 μL aliquot from an overnight cultures of B. subtilis NCIB 3610 (PKS0207) was inoculated into the center of each plate. Residual liquid was left to adsorb into the agar, and the plates were then incubated at 30°C. Two days of incubation was sufficient to see abundant growth of *S.* Mg1, and lysis of B. *subtilis* was observable beginning on day 3.

Extraction of *S.* Mg1 Metabolites from Agar Plates

Wild-type and Δ*lnyI* strains of *S.* Mg1 were cultured on GYM plates (10^5 spores per plate, 30°C) for 2 days. The agar media, with embedded *S.* Mg1, was cut into 1 cm squares and extracted with 100 ml EtOH (30°C, 30 minutes, shaking) followed by 100 ml MeOH. The extracts were pooled and concentrated under reduced pressure. The residues were redissolved in a small volume of MeOH and insoluble precipitates were removed by centrifugation. The supernatants were transferred to screw-cap vials and evaporated to dryness. The residues were redissolved to a final volume of 500 μl in MeOH.

LC-MS for MS/MS Networking of *S.* Mg1 Metabolites

To construct MS/MS networks, combined MS and data-dependent MS/MS LC-MS spectra of wild-type and Δ*lnyI S.* Mg1 extracts were collected as follows. An Agilent 1200 HPLC equipped with a thermostatted autosampler, binary pump, thermostatted column compartment, and UV-Vis DAD detector controlled by HyStar 3.2 SR2 was attached to a Bruker MicroTOF operated by Compass 1.3 for micrOTOF SR1. A Sigma SUPELCOSIL LC-18-T HPLC Column (3.0 x 150 mm, 3 μm) was equilibrated with 72% 10 mM NH_4HCO_3 pH 7 (solvent A) and 28% ACN (solvent B) flowing at 0.4 ml/min with the temperature held at 37°C. Extracts were injected (20 μl) onto the column and eluted with a gradient program: 1) wash postinjection 72:28% (solvent A:B) 2 min, 2) ramp to 68:32% over 1 min, 3) hold at 68:32% for 17 min, 4) ramp to 65:35% over 5 min, 5) hold at 65:35% for 15 min, 6) ramp to 55:45% over 10 min, 7) hold at 55:45% for 8 min, 8) ramp to 35:65% over 5 min, 9) hold at 35:65% for 7 min, 10) ramp to 72:28% over 2 min, 11) reequilibrate with 72:28% for 8 min. Mass spec acquisition parameters: positive mode, mass range *m/z* 200-4000, ESI source (end plate offset: -500 V, capillary: -4500 V, nebulizer: 3.0 bar, dry gas: 10.0 l/min, dry temp: 200°C), ion transfer (funnel 1 RF: 300 Vpp, funnel 2 RF: 400 Vpp, hexapole RF: 180 Vpp), quadrupole for mass selection (ion energy: 8.0 eV, low mass

cutoff: 250 m/z), collision cell (energy: 8.0 eV, transfer time: 80.0 μs, collision RF: 150 Vpp, pre-pulse storage: 8.0 μs), data-dependent MS^2 (select 10 highest precursor ions with minimum threshold of 2000 absolute counts or 5% relative intensity, smart exclusion enabled, active exclusion enabled where precursors are excluded for 1 minute after three MS^2 spectra are acquired). Each run was calibrated (HPLC method) by post-run injection of a NaOAc standard.

MS/MS Network Construction
The MS and MS/MS datasets for the extracts were uploaded to GNPS (http://gnps.ucsd.edu) and molecular networks were generated (Nguyen et al., 2013; Watrous et al., 2012). The wild-type *S.* Mg1 extract dataset was assigned to group 1 and the Δ*lnyI* dataset to group 2. Two types of networks were generated and visualized with Cytoscape (Shannon et al., 2003): a dense network with many node connections to linearmycin variants (minimum cosine threshold: 0.75, network topK: 18, max network size: 200, minimum number of matched peaks: 6, minimum cluster size: 3, cosine-weighted force-directed layout) and a sparse network allowing for easy identification of the most similar variants (minimum cosine threshold: 0.85, network topK: 10, max network size: 100, minimum number of matched peaks: 6, minimum cluster size: 2, FM3 layout).

Isolation of Vesicles
Streptomyces sp. Mg1 wild type, Δ*lnyI*, and Δ*lnyI*+*lnyI* were cultured aerobically in buffered MYM media (250 ml cultures, 30°C, shaking at 200 rpm, light excluded) for 5 days. The mycelia were removed by filtration through Whatman #3 qualitative circles. Filtrates were further clarified of cell particulates by centrifugation (10,800 x g, 30 min, 4°C). The supernatants were filtered (0.22 μm, PES membrane) and vesicles were recovered by ultracentrifugation as follows. Each supernatant was divided into 2 x 94 ml portions and sealed in polyallomar ultracentrifuge tubes (38 x 102 mm, thinwall) with aluminum caps. The samples were ultracentrifuged in a Beckman Type 45 Ti rotor (235,000 × g, 4°C, 2 h). Supernatants were decanted and pellets were resuspended in buffer A (10 mM HEPES, 0.85% w/v NaCl, pH 7.4, sterile-filtered). Two biological repeats of vesicle isolation were performed, each with consistent results.

For further purification of vesicles, pellets were resuspended in a high-density iodixanol solution (50% w/v in buffer A, 1 ml). The high-density layer was then overlaid with lower-density iodixanol solutions [45 (2 ml), 40 (2 ml), 35 (2 ml), 30 (2 ml), 25 (2 ml), 20 (2 ml), and 10% (1 ml) iodixanol in buffer A] to form a step gradient (14 ml total) in Ultra-Clear (14 x 89 mm) ultracentrifuge tubes. The gradients were ultracentrifuged in a SW 41 Ti rotor (100,400 × g, 4°C, 16 h). Fractions (1 ml) were recovered from the top of the gradient, diluted with 3 ml buffer A, and ultracentrifuged in a TLA-100.3 rotor (120,000 × g, 4°C, 45 min). Pellets were resuspended in 500 μl buffer A and stored at 4°C in amber tubes. Fractions were screened for the presence of particles by dynamic light scattering. Repeated vesicle purifications and fractionations yielded similar results in several independent experiments by three different researchers.

EM of Vesicles
For electron microscopic analysis, 2-5 μl of the vesicle preparations were adsorbed onto freshly glow-discharged carbon-coated Formvar grids, washed briefly with water, and negatively stained with a 2% w/v aqueous solution of ammonium molybdate. The samples were observed in a JEOL 1200 EX transmission electron microscope operated at an acceleration voltage of 100 kV. Electron micrographs were recorded at calibrated magnifications using a 3k slow-scan CCD camera (model 15C, SIA). Image analysis was carried out with ImageJ (Schneider et al., 2012). Four fractions from the gradient isolation of vesicles were first screened. Micrographs were recorded from each fraction. The majority of vesicles were observed in the middle fractions. Parallel samples were observed from the Δ*lnyI* mutant, which had few vesicle-like particles and debris.

LC-MS Analysis of Vesicles
For LC-MS analysis of the vesicles an analytical (2.1 x 150 mm, 3 μm, 120 Å) Thermo Scientific Acclaim 120 C18 column attached to a Thermo Scientific Orbitrap Exactive LC-MS was equilibrated with 90% water/0.1% formic acid (solvent A), 10% ACN (solvent B) flowing at 0.2 ml/min. Vesicle preparations were injected (20 μl) onto the column and eluted with a gradient program: 1) wash postinjection 90:10% (solvent A:B) 2 min, 2) ramp to 64:36% over 8 minutes, 3) ramp to 56:42% over 15 minutes, 4) ramp to 35:65% over 7 minutes, 5) hold at 35:65% 5 minutes, 6) ramp to 15:85% over 2 minutes, 7) hold at 15:85% for 5 minutes, 8) ramp to 0:100% over 6 minutes, 9) hold at 0:100% for 2 minutes, 10) ramp to 90:10% over 1 minute, 11) reequilibrate with 90:10% for 5 minutes. Mass spec acquisition parameters: HESI source (spray voltage: 4800 V, capillary temp: 250°C, sheath gas: 40, aux gas: 20, max spray current: 100 μA, heater temp: 200°C), tune settings (capillary: V, tube lens: 185 V, skimmer: 46 V, RF0 DC offset: 12 V, lens 1: 0 V, MP0 and MP1 RF: 700 V, RF1 DC offset: 7 V, MP2 and MP3 RF: 700 V, gate lens: 6.75 V, c-trap RF: 2400 V), Orbitrap mass analyzer (extraction time: 2 Hz, AGC target: 1 × 10^6, injection time: 50 ms, 2 microscans per scan, calibrated with LTQ ESI positive and negative ion calibration solutions from Pierce), scan 1 (positive mode, mass range: 200-2200 m/z), scan 2 (positive mode, mass range: 60-1200 m/z, collision cell: HCD 50 eV). Spectra were selected and processed using Xcalibur.

Time Course Experiment
To observe growth, *lny* gene expression, and vesicle production over time, independent 25 ml buffered MYM cultures were inoculated with a 100 μl suspension containing 5 x 10^7 spores of *S.* Mg1 wild type or Δ*lnyI*. At 12, 24, 36, 48, 72, and 96 h one culture each of wild type and Δ*lnyI* were harvested. At the specified collection time, the culture flask was shaken to resuspend the mycelia. Aliquots

of 1 ml each were removed from the culture, centrifuged at 21,130 x g for 10 min to pellet the mycelia, and stored dried at -20°C for later growth measurements. After collecting aliquots for growth measurements, the remainder of the cultures was centrifuged at 12,000 × g for 10 min at 4°C. The mycelial pellets were fixed with RNA-protect Bacteria Reagent (Qiagen) and stored at -80°C for later RNA extraction. The culture supernatants were immediately processed for vesicle purification, as described below.

Growth Measurements

The growth of *S.* Mg1 was determined using a previously described diphenylamine colorimetric method (Zhao et al., 2013). Briefly, mycelial pellets were washed twice with phosphate-buffered saline, resuspended in 1 ml of diphenylamine reagent [1.5% w/v diphenylamine, 1.5% v/v sulfuric acid, and 0.008% v/v aqueous acetaldehyde in glacial acetic acid], and incubated at 60°C for 1 h. After incubation, samples were centrifuged at 21,130 × g for 5 min and the absorbance at 595 nm was measured from 200 μl of the supernatant. Ungerminated spores, at an identical density used to inoculate the cultures, were used to measure the 0 hour time point.

Time Course Vesicle Extraction, Purification, and EM

Vesicles were isolated similarly, as above, with the following modifications for smaller culture volumes: supernatants were treated with 0.1 mg of DNase I for 15 min, filtered (0.22 μm, PES membrane), and ultracentrifuged for 3 h, as above. The pellets were resuspended in an iodixanol solution (50% w/v in Buffer A, 200 μl) and overlaid with lower-density iodixanol solutions [50 (200 μl), 40 (400 μl), 30 (400 μl), 20 (400 μl), 10 (400 μl), and 0% (100 μl) in Buffer A] to form a step gradient (2.1 ml total) in Ultra-Clear (11 x 34 mm) ultracentrifuge tubes. The gradients were ultracentrifuged to equilibrium in a TLS55 rotor (120,000 × g, 4°C, 16-18 h). Fractions (200 μl) were recovered from the top (fraction 1) to the bottom (fraction 10) of the tube and stored at 4°C. To remove iodixanol for subsequent EM analysis, 100 μl each of fractions 5 and 6 were pooled, diluted to 2.1 ml with Buffer A in Ultra-Clear (11 x 34 mm) ultracentrifuge tubes, ultracentrifuged (120,000 × g, 4°C, $\geq$ 6 h), and the pellet was resuspended in 30 μl of Buffer A. For EM, 3 μl of each vesicle preparation was stained and observed as above.

Plate Overlay Lysis Assays and LC$_{50}$ Measurement

To assay vesicle fractions for lytic activity, we adapted a previously described plate assay (Stubbendieck and Straight, 2015). Briefly, overnight cultures of B. subtilis were diluted to OD$_{600}$ = 0.08 in 25 ml of MYM. When the cultures reached stationary phase, the cells were concentrated to OD$_{600}$ = 4 by centrifugation at 3220 × g for 5 min and resuspension in a reduced volume of MYM. For each plate, 1.5 ml of concentrated B. subtilis was mixed with 4.5 ml of MYM agar (0.67% w/v) and spread evenly over the 25 ml MYM plate. Once the top layers solidified, 3 μl of each vesicle fraction was directly spotted onto the overlay and allowed to dry before the plates were incubated at 30°C. After 18 h plates were photographed or scanned.

To compare lytic activity from vesicles extracted at different time points, equal volumes of vesicle fractions 5 and 6 were pooled, serially diluted two-fold, and spotted onto plates, as above. After incubation, plates were scanned and the mean pixel intensity (MPI) of each lysed spot was determined using ImageJ. The ratio of MPI of each serial dilution relative to the fully concentrated sample was calculated, natural log-transformed, and plotted against the dilution factor. Data points whose MPI ratios were $\geq$ 0.95 or $\leq$ 0.39 were not plotted because these values indicate assay saturation and background, respectively. For each vesicle preparation, the LC$_{50}$ value was determined by calculating the dilution where the ratio of MPI = 0.67, which represents the middle point between saturation and background intensity ratio. All linear regressions used 3 or 4 data points and the LC$_{50}$ values were within the interpolable range. All R^2 values were $\geq$ 0.99.

Quantification of Linearmycin in Vesicle Preparations

To quantify linearmycins in vesicles, 3 μl each of fractions 5 and 6 were pooled and linearmycins were extracted with 6 μl of methanol. A 6 μl sample was injected onto an Agilent 1200 HPLC system with a Phenomenex Luna C$_{18}$ column (4.6 x 250 mm, 5 μm) and eluted with an 20 mM ammonium acetate pH 5 (solvent A)/ACN (solvent B) gradient flowing at 1 ml/min. The elution program was as follows: 1) 60:40% (solvent A:B) 5 min,2) ramp to 50:50% over 10 min, 3) ramp to 25:75% over 5 min, and 4) ramp down to 60:40% ACN over 5 min (Stubbendieck and Straight, 2015). Peaks primarily consisting of linearmycins A and B were detected by UV absorbance at 333 nm with retention times of 13 and 16 min, respectively.

RNA Extraction and Cleanup

To extract RNA, five 3 mm glass beads and 2 ml of ice-cold lysis buffer [4 M guanidine thiocyanate, 25 mM trisodium citrate dihydrate, 0.5% w/v sodium N-lauroyl sarcosinate, and 0.8% v/v β-mercaptoethanol] were added to each fixed mycelial pellet. After 2 min of vortexing, 2 ml of TRI Reagent (Sigma-Aldrich) was added to each sample. Samples were then vortexed in four cycles of 30 s on vortex and 30 s on ice. After the addition of chloroform, RNA was extracted following standard procedures. Trace DNA was removed from the RNA samples using a Turbo DNA-free kit (Applied Biosystems).

Quantitative RT-PCR

Complementary DNA was reverse transcribed from 100 ng of total RNA using a High-Capacity RNA-to-cDNA Kit (Thermo Fisher Scientific). Quantitative PCR was performed using a Sso Advanced Universal SYBR Green Supermix Kit (Bio-Rad) and a CFX96 Touch real-time PCR thermocycler (Bio-Rad) with the following cycling parameters: denaturation at 95°C for 30 s; 40 cycles of denaturation at 95°C for 15 s, annealing at 58°C for 30 s, and extension at 72°C for 30 s; followed by a final melting curve from 60°C to 95°C

for 6 min. We amplified *lnyHA* and *lnyHI*, the first and last PKS-encoding open-reading frames, respectively using primers RMSq21-22 and RMSq23-24 (Tables S2 and S3). Each reaction was run in triplicate and using LinReg (Ruijter et al., 2009) we calculated the primer efficiency and quantification cycle values. All values are reported as fold difference compared to 24 h.

Vesicle Quantitation

Using ImageJ, we counted, outlined, and measured the cross-sectional area of membranous particles in EM images of vesicle preparations from *S*. Mg1 grown for 72 h. We analyzed two independent matched vesicle preparations from *S*. Mg1 wild type and Δ*lnyI*. For one set of vesicle preparations, we analyzed EM images of two fields each of wild type and Δ*lnyI*. In the replicate set of vesicle preparations, we analyzed EM images of four fields each of wild type and Δ*lnyI*. In total, we counted and measured 1413 particles in six fields each from both strains. Each field was 50 μm^2. We plotted histograms in R (R Core Team, 2013) using the ggplot2 package (Wickham, 2009).

Surfactin Test

The 24 h samples were chosen for this test because the lytic activity in the concentrated vesicle preparations was nearest the saturation point, allowing a dynamic range of dilutions from lytic to no detectable activity. To test the effect of exogenous surfactin on vesicle preparations, vesicles were extracted from *S*. Mg1 cultures after 24 h and serially diluted two-fold in Buffer A containing a 2.5 mg/ml mixture of surfactins, in ethanol, isolated from *B. subtilis* (Sigma). Lysis was assayed as above (see "Plate Overlay Lysis Assays and LC_{50} Measurement").

QUANTIFICATION AND STATISTICAL ANALYSIS

Statistical details and information about replication can be found in the corresponding figure legends for each experiment.

Supplemental Information

A Link between Linearmycin Biosynthesis and

Extracellular Vesicle Genesis Connects Specialized

Metabolism and Bacterial Membrane Physiology

B. Christopher Hoefler, Reed M. Stubbendieck, N. Kalyani Josyula, Sabrina M. Moisan, Emma M. Schulze, and Paul D. Straight
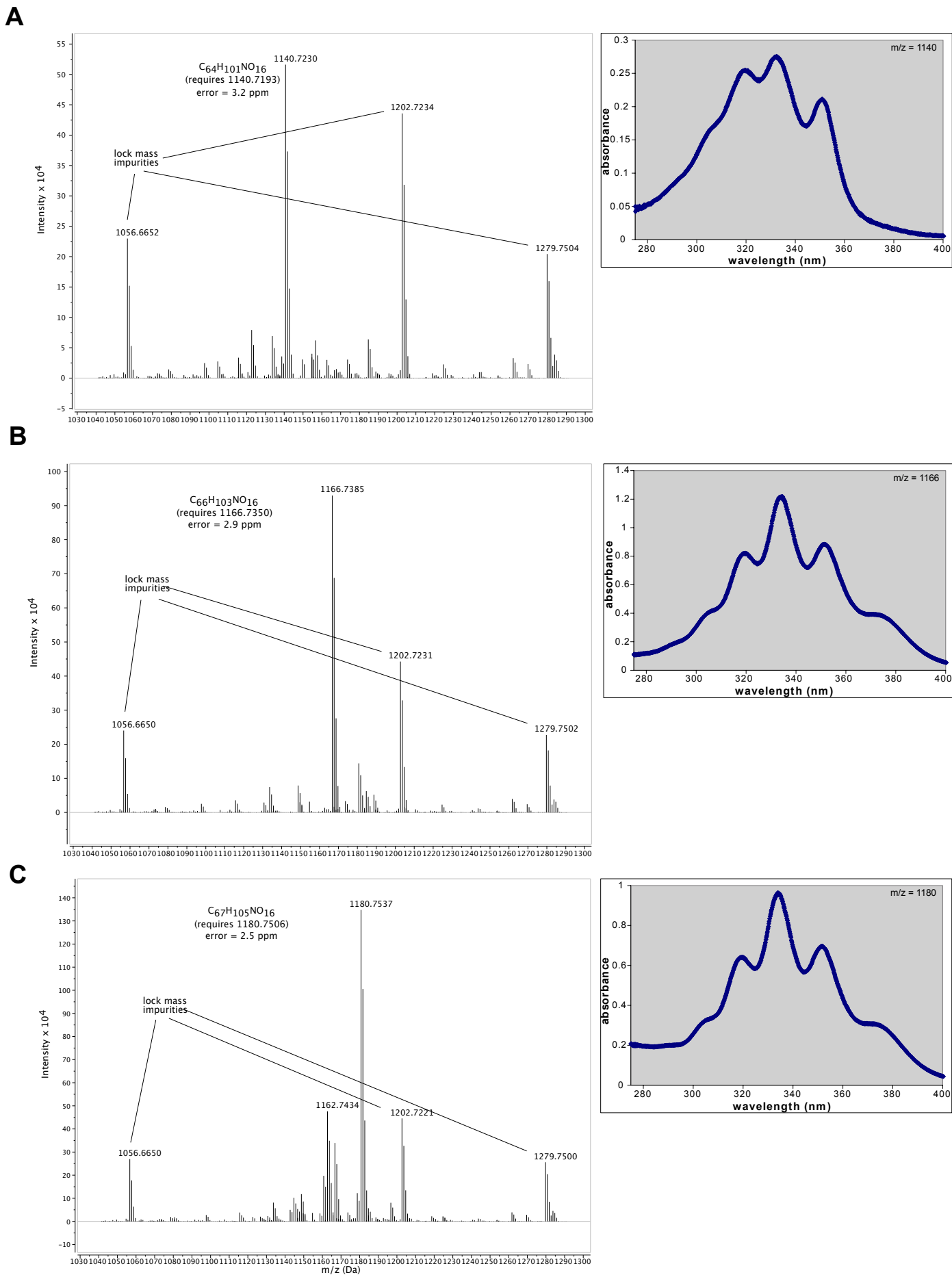
Figure S1. Relates to Figure 1. (A) MS2 spectra with fragment analysis (left) and UV-Vis spectra of 10μg/ml solutions in MeOH (right) of : (A) Linearmycin A (B) Linearmycin B (C) Linearmycin C.
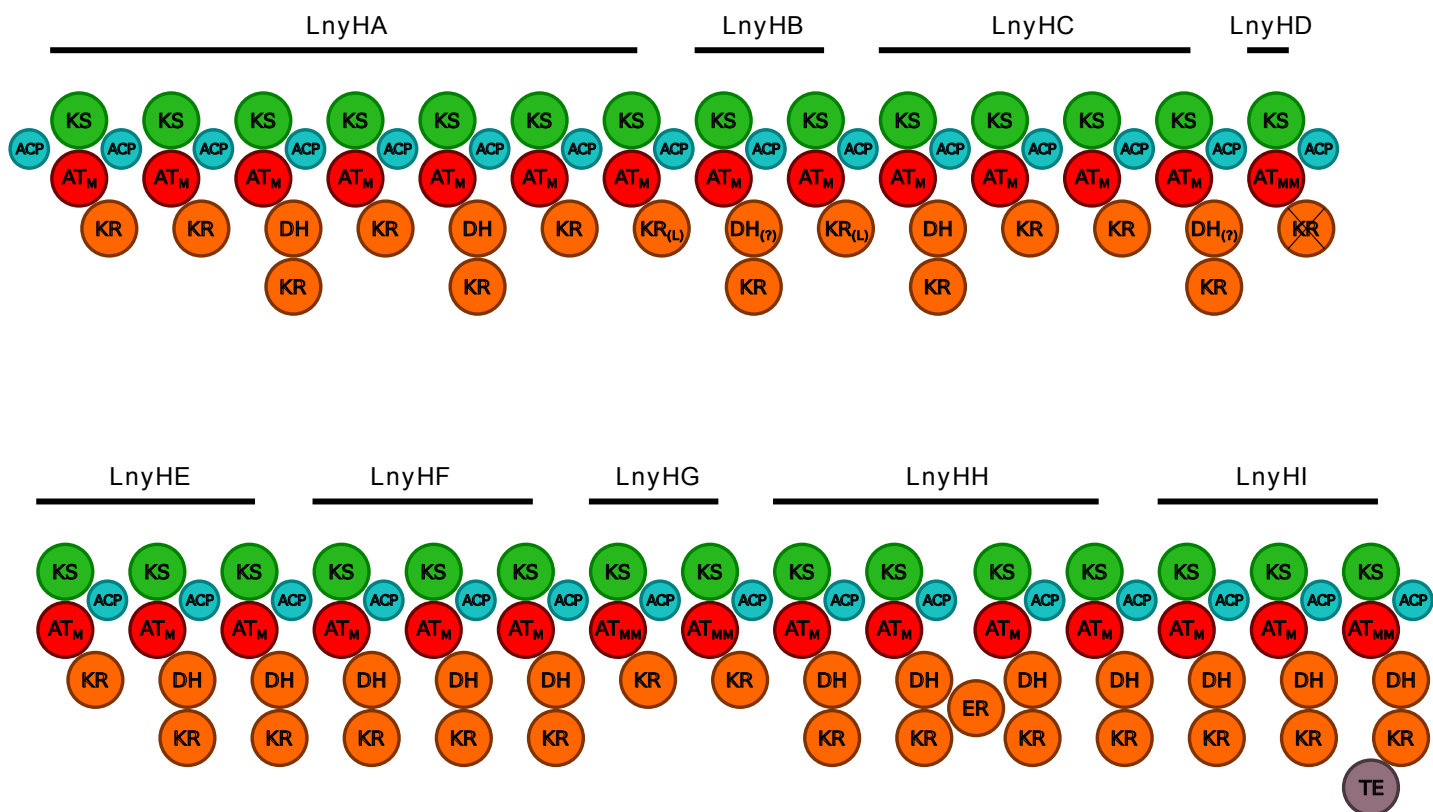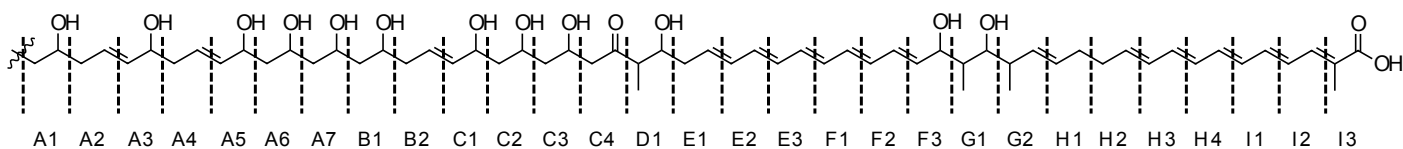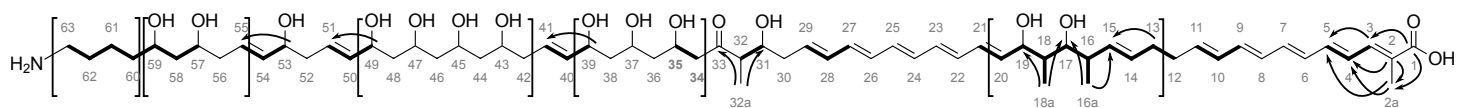
Figure S2. Relates to Figure 1 and Table S4. A. Polyketide synthase domain analysis of the *lny* gene cluster from *S*. Mg1. B. Predicted backbone structure based on domain analysis. C. Linearmycin C structure with significant NMR correlations highlighted. Solid black lines: COSY and/or H2BC, brackets: HSQC-TOCSY, arrows: HMBC.
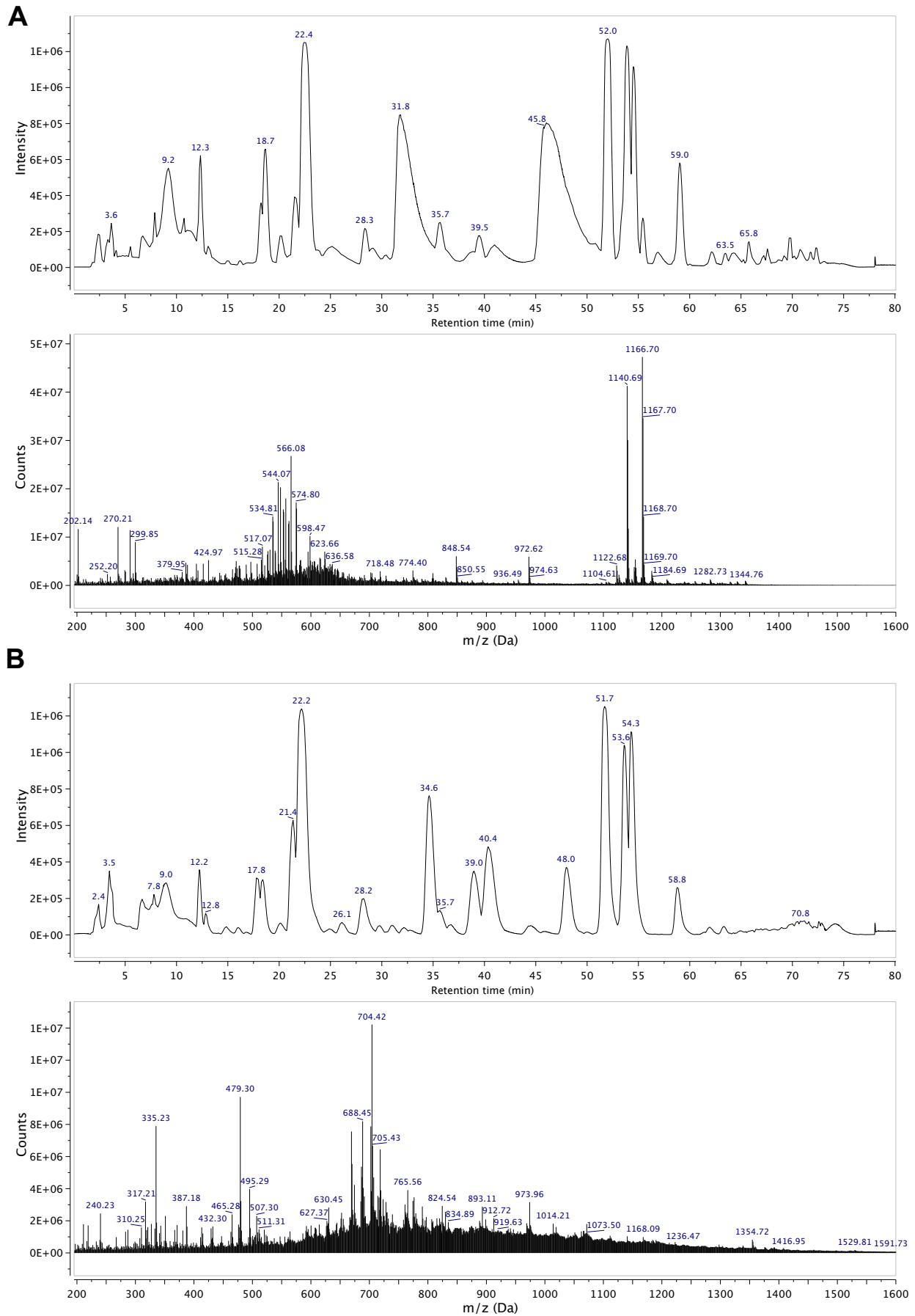
Figure S3. Relates to Figure 2. LC-MS analysis of (A) wild type and (B) Δ*lnyI* S. Mg1 extracts. For each sample, top- base peak chromatograms, and lower- averaged MS^1 spectra from 25-51 minutes.
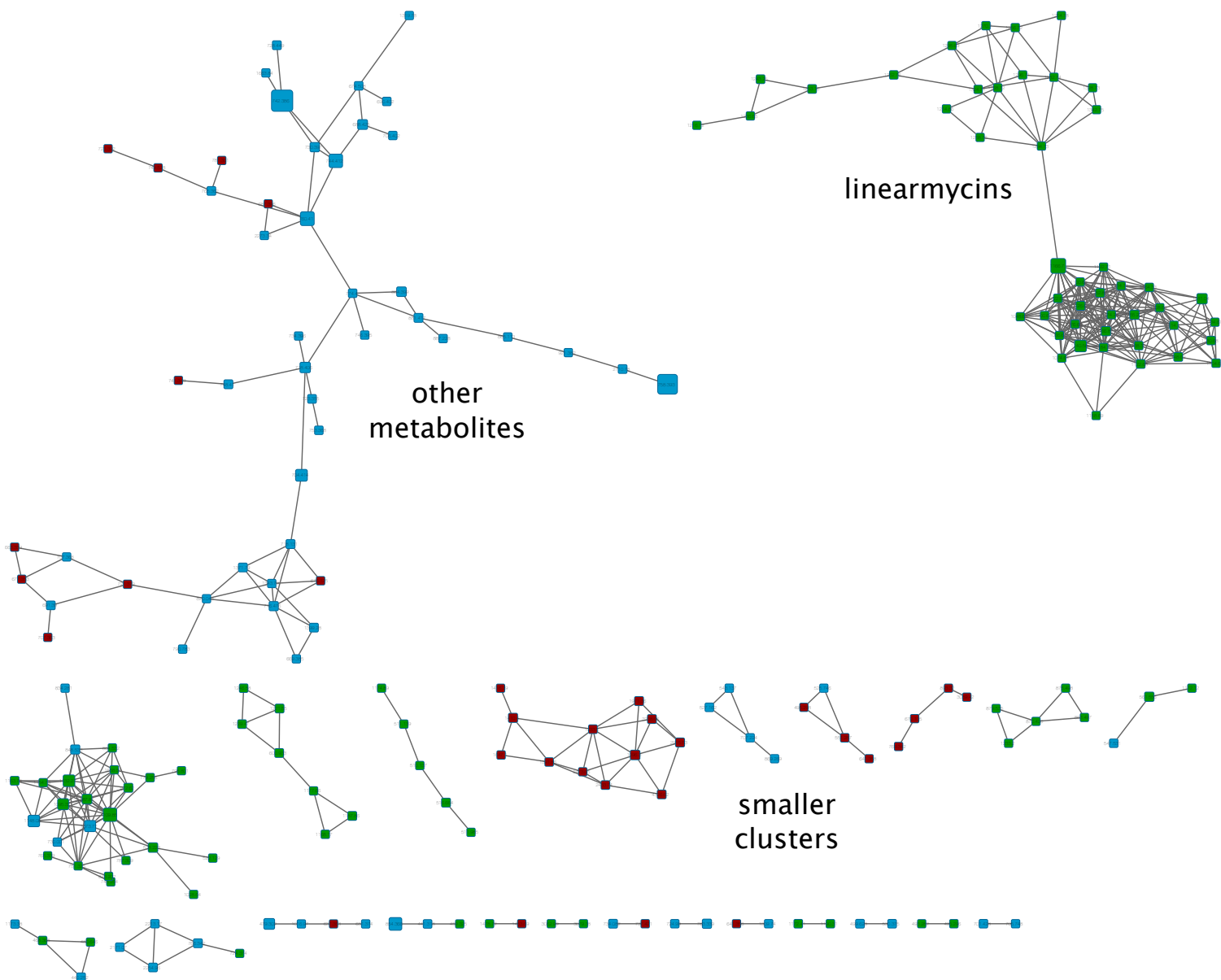
Figure S4. Relates to Figure 3. Complete MS/MS network of wild-type and Δ*lnyI S.* Mg1 extracts. Each node represents one MS1 precursor ion. Nodes are colored GREEN if observed only in wild-type extracts, RED if observed only in Δ*lnyI* extracts, and BLUE if observed in both extracts. Nodes are connected if the MS/MS similarity has a cosine score of 0.75 or greater. Node sizes are scaled relative to the precursor ion intensity.
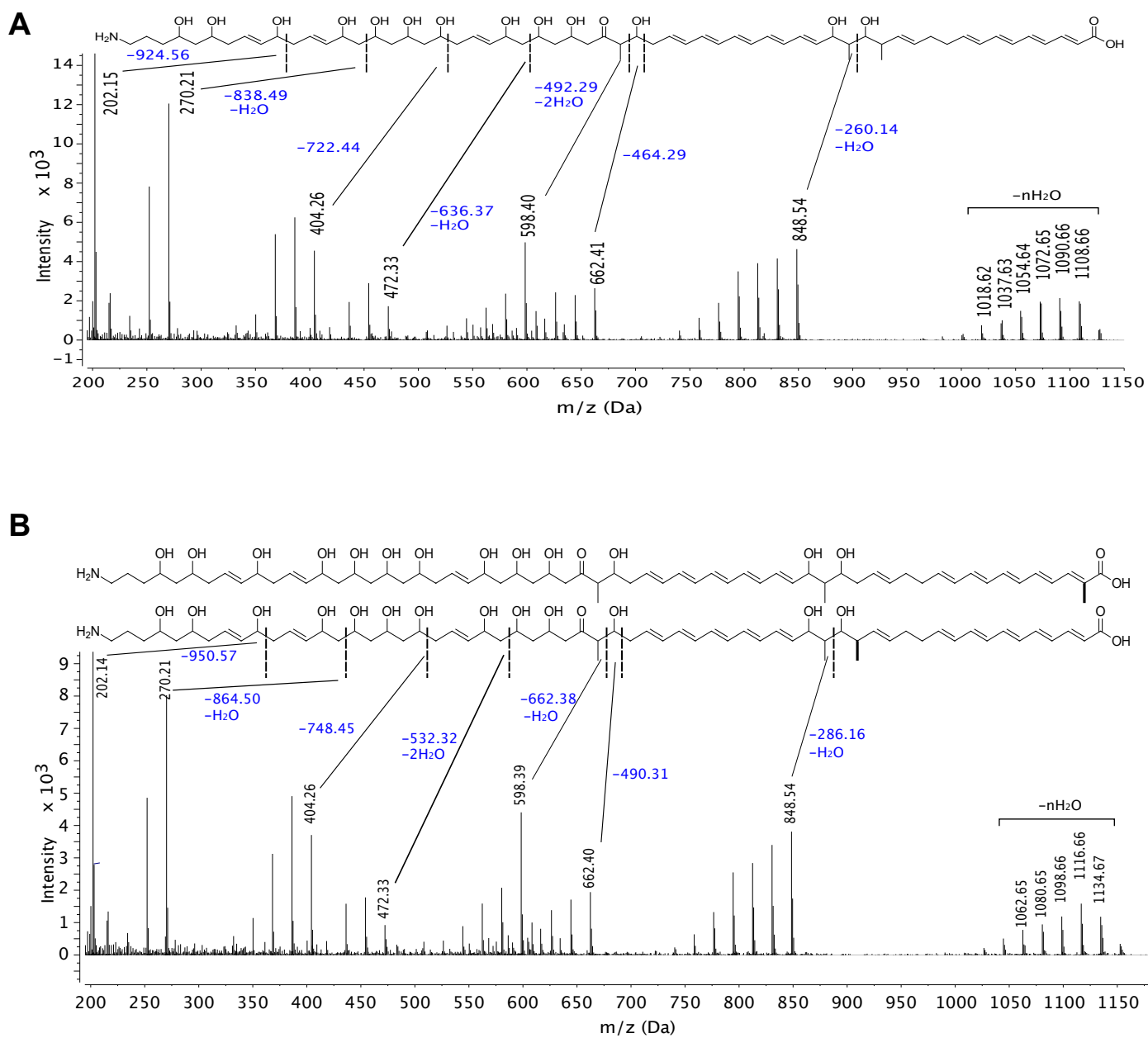
Figure S5. Relates to Figure 3. Predicted linearmycin variant forms from MS2 fragment analysis. (A) MS2 spectrum and fragment analysis of m/z 1126 representing premature chain termination products. (B) MS2 spectrum and fragment analysis of m/z 1152 representing incorporation of malonyl-CoA in the place of methylmalonyl-CoA at one of two possible locations (indicated by loss of methyl group in either structure).
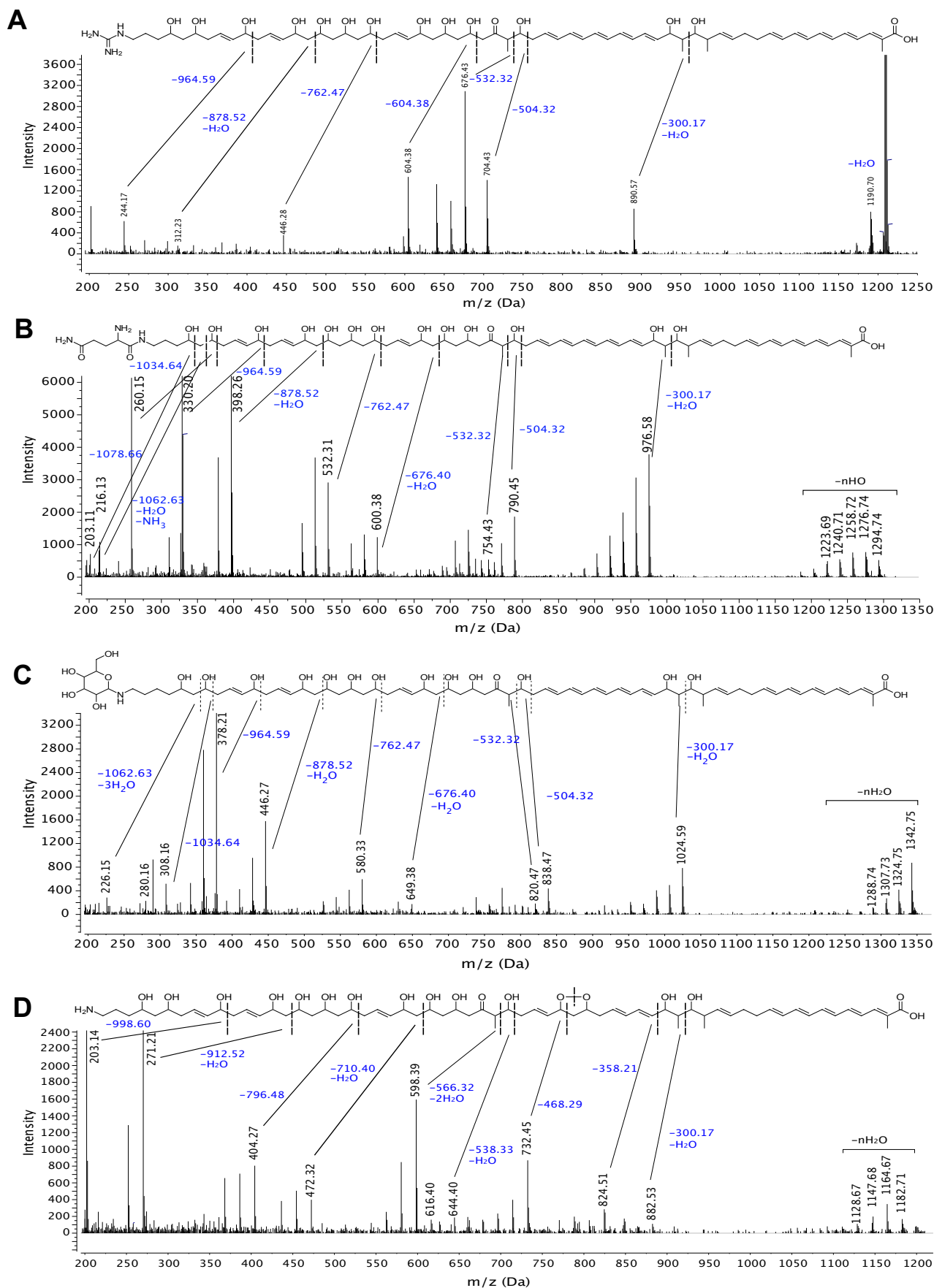
Figure S6. Relates to Figure 3. Predicted linearmycin variant forms from MS2 and fragment analysis. (A) *m/z* 1126 representing initiation from a guanidino-containing starter unit. (B) *m/z* 1152 representing modification of the starter unit with glutamine. (C) *m/z* 1342 representing modification of the starter unit with glucose. (D) *m/z* 1200 representing oxidized linearmycin variants.
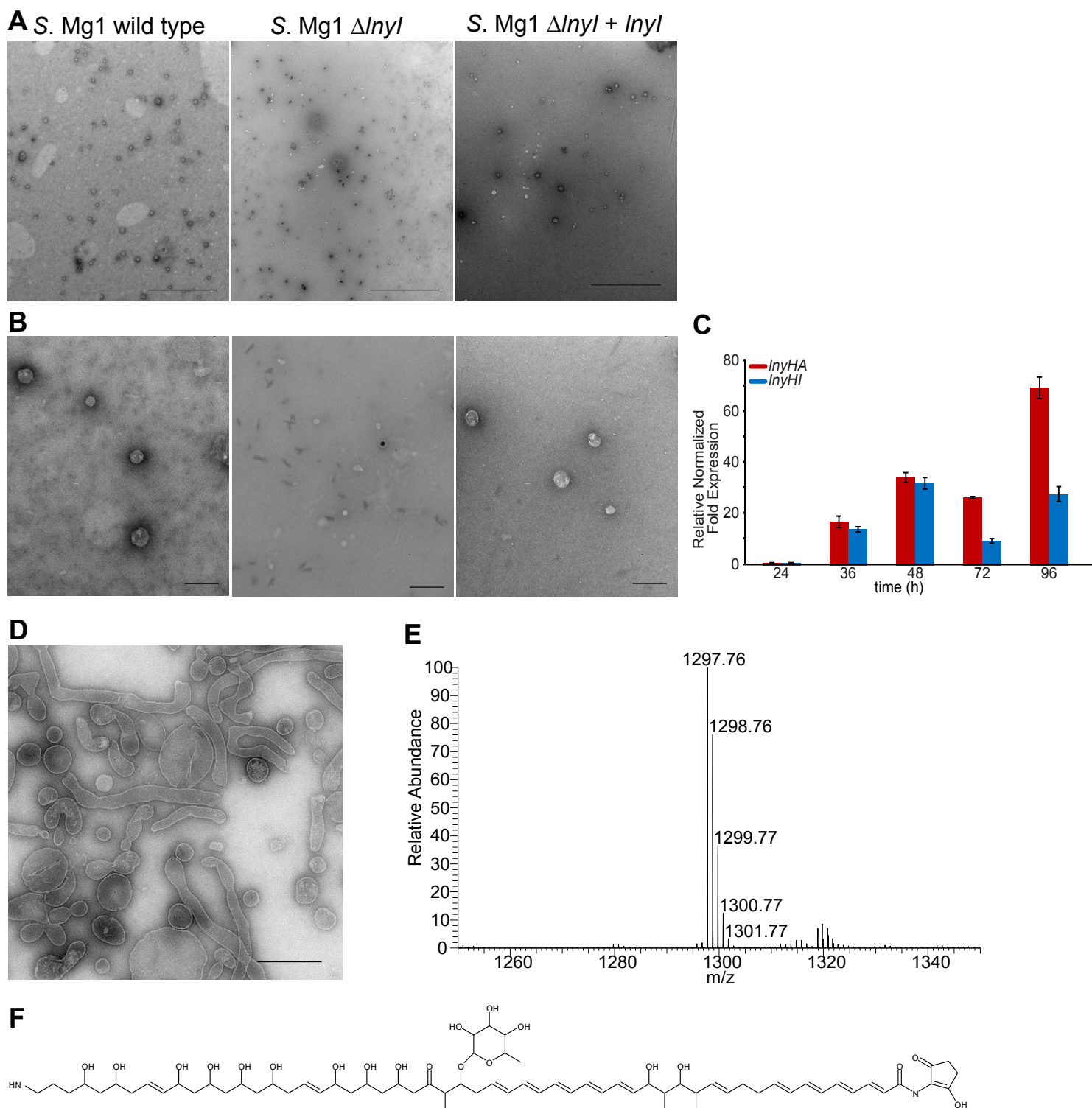
Figure S7. Relates to Figures 4 and 5. (A and B) Extra cellular vesicles collected from equivalent gradient fractions from wild type, Δ*lnyI*, and Δ*lnyI*/*lnyI*+ strains. (A) Lower magnification fields, scale bar is 2 μm. (wild type: 55 ± 4.4, 75-200 nm, Δ*lnyI*: 2.3 ± 2.5, 75-200 nm, and Δ*lnyI*/*lnyI*+ 27.3 ± 2.5, 75-200 nm particles per field). (B) Higher magnification fields, scale bar is 0.2 μm. (C) Quantitative RT-PCR was used to determine the relative fold expression in S. Mg1 wild type for *lnyHA* and *lnyHI* within the *lny* gene cluster at the specified times. The error bars represent the standard deviation of the fold difference. The expression of *hrdB* is greatly diminished at 96 hours as cultures enter stationary phase, which produces an artificial elevation of the normalized 96 hour sample. Earlier than 96 hours, the expression pattern over time is unchanged with or without *hrdB* normalization. (D-F) Isolation of ECO-02301 containing vesicles from *S. aizunensis*. (D) EM micrograph of vesicle-containing gradient fraction from supernatant of *S. aizunensis* culture. Vesicles and membranous tubular structures are observed. Scale bar is 0.2 μm. (E) MS of ECO-02301 extracted from isolated vesicle fractions of *S. aizunensis*. (F) The structure of ECO-02301, MW = 1297.7 (McAlpine et al, 2005).

Table S1. Strains used in this study, Related to STAR Methods.

Strain	Genotype	Source
PSK0207	*Bacillus subtilis* NCIB 3610	[Branda et al., 2001]
PSK0558	*Streptomyces sp.* Mg1	[Barger et al., 2012]
PDS0116	*Streptomyces aizunensis* NRRL B-11277	USDA
PDS0067	*B. subtilis* NCIB 3610 Δ*pksX::spc*	[Barger et al., 2012]
PSK0049	*B. subtilis* NCIB 3610 Δ*srfAA::mls*	[Branda et al., 2001]
PDS0755	*Streptomyces sp.* Mg1 Δ*lnyI::apr*	This study
PDS0794	*Streptomyces sp.* Mg1 Δ*lnyI:apr attB::lnyI* (*hyg*)	This study
BW25113	*E. coli* F⁻ *Δ(araD-araB)567 ΔlacZ4787*(::rrnB-3) λ⁻ *rph-1 Δ(rhaD-rhaB)568 hsdR514*	Coli Genetic Stock Center
EC100	*E. coli* F⁻ *mcrA* Δ(*mrr-hsdRMS-mcrBC*) φ80d*lacZ*ΔM15 Δ*lacX74 recA1 endA1 araD139 Δ(ara, leu)7697 galU galK* λ⁻ *rpsL nupG*	Epicentre
WM3780	*E. coli dam-3 dcm-9 metB1 galK2 galT27 lacY1 tsx-78 supE44 thi-1 mel-1 tonA31 attHK*::pJK202*Δ(oriR6K-aadA)*::Frt	[Blodgett et al., 2005]

Table S2. Primers used in this study, Related to STAR Methods.

Primer	Sequence (5'- 3')
SM066	TCTGTGACGCCTTCAACATC
SM067	GTACAGCTTGGTGGCGATCT
SM080	TCACAGCATCCCGGAAGCAAAGGTATTTCACGGATCATGattccggggatccgtcgacc
SM081	CCCGGCCCCGTTCGCTCTGTTCGCTCCGTCAGGCCGTCAtgtaggctggagctgcttc
EMH029	GATCCGCGGCCGCGCGCGATgctggttccaggtgctgtg
EMH030	GACATGATTACGAATTCGATctctgttcgctccgtcagg
BCH0166	GCAAATTCCTGATGCTCGAC
BCH0167	CTCACGGGCCCGCTTCTT
RMSq21	CTGCCTTCGTACCCGTCATG
RMSq22	TGCGACCAGTTCACCTTCAG
RMSq23	CCTCGTCGACATCTACTCGC
RMSq24	AGTCGAAGAACTGCTCCTGC

Note: lower case indicates target differences for recombination-specific procedures (see methods).

Table S3. Annotated open reading frames of the linearmycin gene cluster, Related to Figure 1 and Figure S2.

Accession #	Start	Stop	Product	Gene
AKL64821.1	1062308	1061319	agmatinase	*lnyT*
AKL64822.1	1063971	1062415	methylmalonyl-CoA carboxyltransferase	*lnyS*
AMB20391.1	1064457	1067375	transcriptional regulator	*lnyR*
AKL64823.1	1067356	1068252	metallophosphoesterase	*lnyQ*
AKL64825.1	1069184	1070845	amine oxidase	*lnyO*
AKL64826.1	1072351	1070939	acyl--CoA ligase	*lnyN*
AKL69762.1	1073028	1072435	thioesterase	*lnyM*
AMB20392.1	1073738	1073166	glucose-1-phosphate thymidylyltransferase	*lnyL*
AKL64827.1	1074063	1075127	daunorubicin ABC transporter ATPase	*lnyK*
AKL69763.1	1075226	1075996	ABC transporter	*lnyJ*
AKL64828.1	1076160	1077197	acyltransferase	*lnyI*
AMB20393.1	1094107	1077302	polyketide synthase	*lnyHI*
AKL64829.1	1116644	1094175	polyketide synthase	*lnyHH*
AKL64830.1	1126318	1116707	polyketide synthase	*lnyHG*
AKL64831.1	1142603	1126413	polyketide synthase	*lnyHF*
AMB20394.1	1158345	1142689	polyketide synthase	*lnyHE*
AKL64832.1	1163497	1158599	polyketide synthase	*lnyHD*
AKL64833.1	1183653	1163620	polyketide synthase	*lnyHC*
AKL69764.1	1193985	1183678	polyketide synthase	*lnyHB*
AKL64834.1	1228586	1194150	polyketide synthase	*lnyHA*
AKL64835.1	1230452	1228902	membrane protein	*lnyG*
AKL69765.1	1230949	1230449	membrane protein	*lnyF*
AKL64836.1	1231545	1231012	hypothetical protein	*lnyE*
AKL64837.1	1231711	1233006	histidine kinase	*lnyD*
AKL69766.1	1233071	1233631	LuxR family transcriptional regulator	*lnyC*
AKL69767.1	1236565	1233701	transcriptional regulator	*lnyB*
AKL64838.1	1237554	1236790	Thioesterase	*lnyA*

Table S4. Linearmycin C ^{1}H and ^{13}C NMR assignments, Related to Figure 1 and Figure S2.

C #	^{13}C (ppm)	^{1}H (ppm)	J_{HC} (Hz)	COSY	H2BC	HMBC	TOCSY
1	177.60	-	-	-	-	2a,3	-
2	135.56	-	-	-	-	2a,4	-
2a	14.44	1.94	128		3	3,4,5	
3	134.83	7.01	152	4	4	5	
4	130.20	6.52	152	5	3,5		
5	137.51	6.47	156	6	4,6		
6	133.85	6.35	147		5,7		
7	135.67	6.35	147	8	6,8		
8	132.36	6.26	147		7,9		
9	135.18	6.26	154	10	8,10		
10	132.50	6.14	140	11	9,11		
11	136.26	5.77	152	12	10,12		
12	34.11	2.22	128	13	11,13		13-21
13	33.51	2.15	123	14	12,14	15	
14	131.46	5.48	147	15	13,15		
15	134.45	5.46	147	16	14,16		
16	41.60	2.35	126	17	15,17		
16a	18.54	0.98	126	16	16	15,17	
17	77.85	3.40	142	18	16,18		
18	42.42	1.65	126	19	17,19		
18a	8.77	0.94	126	18	18	17,19	
19	74.99	4.27	144	20	18,20		
20	137.14	5.71	153	21	19,21		
21	131.79	6.27	147		20,22		
22	133.66	6.27	147		22,23		
23	133.81	6.27	147		22,24		
24	134.00	6.28	147		23,25		
25	133.93	6.27	147	26	24,26		
26	132.97	6.22			25,27		
27	134.25	6.22		28	26,28		
28	134.36	6.19		29	27,29		29-35
29	132.05	5.73	156	30	28,30		
30	39.38	2.27	126	31	29,31		
31	72.54	3.96	146	32	30,32		

C #	^{13}C (ppm)	^1H (ppm)	J_{HC} (Hz)	COSY	H2BC	HMBC	TOCSY
32	53.24	2.65	128		31	33	
32a	10.91	1.10	129	32	32	31,33	
33	214.46	-	-	-	-		-
34	49.78	2.69,2.63	121	35		33	35-39
35	67.23	4.24	146	36	34,36		
36	45.20	1.63	121-126		35,37		
37	69.15	3.88	142	38	36,38		
38	45.32	1.68,1.60	121-126		37,39		
39	72.02	4.24	143	40	38,40	41	
40	136.45	5.52	154	41	39,41		
41	129.17	5.71	154	42	40,42		42-49
42	42.01	2.23	126	43	41,43		
43	69.06	3.88	142	44	42,44		
44	45.47	1.59,1.49	121-126		43,45		
45	66.27	4.08	143	46	44,46		
46	46.64	1.54	123		45,47		
47	66.24	4.06	143	48	46,48		
48	46.17	1.59	126		47,49		
49	70.34	4.27	142	50	48,50	51	
50	137.24	5.56	130	51	49,51		
51	127.67	5.66	128	52	50,52		
52	41.45	2.24	126	53	51,53		53,54
53	73.33	4.06	144	54	52,54	55	
54	136.49	5.54	154	55	53,55		
55	128.64	5.68	147	56	54,56		56-60
56	41.49	2.22	126	57	55,57		
57	71.24	3.81	142	58	56,58		
58	44.35	1.56	123		57,59		
59	71.05	3.77	142	60	58,60		
60	23.47	1.54,1.44	118-124	61			61-63
61	28.60	1.66	128	62			
62	37.61	1.54,1.44	118-124	63			
63	40.60	2.92	145				